AN ANGULAR-CORRELATION STUDY OF THE $^{24}Mg(^{3}He, \alpha\gamma)^{23}Mg$ REACTION

by

Larry Carroll Haun

Department of Physics
Duke University

Date: March 4, 1968

Approved:

N. Russell Roberson, Supervisor

A dissertation submitted in partial fulfillment of the requirements for the degree of Doctor of Philosophy in the Department of Physics in the Graduate School of Arts and Sciences of Duke University

1968

ABSTRACT

(Physics)

AN ANGULAR-CORRELATION STUDY OF THE $^{24}Mg(^{3}He, \alpha\gamma)^{23}Mg$ REACTION

by

Larry Carroll Haun

Department of Physics
Duke University

Date: _____

Approved:

_____
N. Russell Roberson, Supervisor

_____

_____

_____

_____

An abstract of a dissertation submitted in partial fulfillment of the requirements for the degree of Doctor of Philosophy in the Department of Physics in the Graduate School of Arts and Sciences of Duke University

1968

AN ANGULAR-CORRELATION STUDY OF THE $^{24}Mg(^{3}He, \alpha\gamma)^{23}Mg$ REACTION

by

Larry Carroll Haun

Nine excited states of ^{23}Mg have been investigated with the $^{24}Mg(^{3}He, \alpha\gamma)^{23}Mg$ reaction at ^{3}He bombarding energies of 6.37 and 8.05 MeV using the angular-correlation method of axial symmetry. The observed α particles were detected in an annular semiconductor counter positioned at 180° relative to the beam direction. From the analysis of the experimental angular correlations, and in conjunction with known ℓ_n values for ^{23}Mg, spin and parity assignments of $5/2^+$, $7/2^{(+)}(3/2)$, $1/2^+$, $9/2^{(+)}(5/2)$, $1/2^-(3/2^-)$, $3/2^-$, $(5/2^+)$, and $1/2^+$ were established for the levels at 0.451, 2.048, 2.356, 2.712, 2.768, 3.792, 3.968, and 4.353 MeV, respectively. Gamma-ray branching ratios were determined for each of these levels as were the γ-ray multipole mixing ratios for most of the transitions. Coincidence measurements performed with a 20.6 cc Ge(Li) detector led to the determination of the decay modes of the 2.712- and 2.768-MeV levels. Yield curves of α particles detected in the

annular counter and leading to the ^{23}Mg ground state and the levels at 0.451, 2.048, and 2.356 MeV were measured for ^{3}He bombarding energies between 6.0 and 8.2 MeV.

The predictions of a strong-coupling collective model are compared with the experimental results. The ground state and the levels at 0.451, 2.048, and 2.712 MeV can be regarded as members of a $K^{\pi} = 3/2^{+}$ rotational band based on Nilsson orbit 7 with the ground state being the band head. The observed mixing and branching ratios for the γ-ray transitions among these levels agree with the model calculations, assuming the levels to be unperturbed by band mixing. A prolate deformation of $\eta \approx 4$ is indicated. The levels at 2.356, 2.904, and 3.968 MeV can be identified as members of a $K^{\pi} = 1/2^{+}$ rotational band based on Nilsson orbit 9 with the 2.356-MeV level being the bandhead. Band mixing between this band and the $K^{\pi} = 3/2^{+}$ band was attempted in order to calculate the mixing and branching ratios for the 2.356- and 2.904-MeV levels. The negative parity levels at 2.768 and 3.792 MeV are possible members of a $K^{\pi} = 1/2^{-}$ rotational band based on Nilsson orbit 4 with the 2.768 MeV level, representing a core-excited state, being the bandhead. The observed level at 3.856 MeV appears to be the third member of this band with $J^{\pi} = 5/2^{-}$. The level at 4.353 MeV can be interpreted as the bandhead of a $K^{\pi} = 1/2^{+}$ rotational band formed by promotion of a core nucleon from Nilsson orbit 6 into orbit 7.

ACKNOWLEDGMENTS

I wish to express my gratitude to Dr. N. R. Roberson who suggested this project and has given his continued interest and support during all phases of this work. I am indebted to Dr. D. R. Tilley for many helpful discussions related to both the measurements and the analysis of the data. I wish to thank Dr. R. V. Poore for his continued help with the computer programming, many helpful discussions concerning experimental problems, his assistance in taking data, and particularly the Ge(Li) detector data which he laboriously took.

The assistance of Drs. V. H. Webb and M. B. Lewis in taking the data is deeply appreciated. I would like to thank Mr. S. E. Edwards for his help with the electronics and Mr. R. L. Rummel and the entire Nuclear Structure Group for the assistance with the accelerator. I am obliged to Mrs. Joseph Bailey who did an excellent job in preparing the illustrations. Thanks are also due to Mr. A. W. Lovette for many helpful suggestions concerning the design of the evaporator.

I would like to thank Dr. E. K. Warburton for the use of his angular correlation code and Dr. A. Waltner for providing the ^{24}Na and

ThC" sources. Special thanks are also due to Dr. R. E. Grove at Randolph-Macon College and Dr. R. H. Rohrer and Mr. R. W. Carter at Emory University who offered much help and encouragement during my academic career. I wish also to thank my parents who have offered continuous encouragement.

I am grateful to Drs. H. W. Newson and E. G. Bilpuch and the Nuclear Structure Laboratory for providing me with the research assistantship. This work was supported in part by the Atomic Energy Commission.

L. C. H.

CONTENTS

LIST OF FIGURES

LIST OF TABLES

AN ANGULAR-CORRELATION STUDY OF THE $^{24}Mg(^{3}He, a\gamma)^{23}Mg$ REACTION

Chapter I

INTRODUCTION

A. General

One of the major contributions to the understanding of nuclear behavior has been the nuclear collective model, for which the formulation was first carried out in detail in 1952 by A. Bohr (1) and was later extended by Bohr and Mottelson (2) and by Nilsson. (3) This model was originally formulated to explain phenomena such as the large static quadrupole moments and enhanced E2 transition probabilities encountered in the study of heavy nuclei. Considerable success was achieved within the atomic mass regions $150 \leq A \leq 190$ and $A \geq 222$.

Nilsson (3) treated quantitatively the behavior of a single particle within the non-spherical potential provided by a deformed core. According to this formulation, the spectra of nuclei having the same odd nucleon number, either N or Z, should be similar. Although this model was not expected to be valid below A = 100, Litherland et al. (4, 5) established in 1956 the applicability of this model to light nuclei in their interpretation of the level

schemes of the mirror pair $^{25}_{13}Al_{12}$ (Z = 13) and $^{25}_{12}Mg_{13}$ (N = 13).

The nuclear systems with N or Z = 11 consist of $^{19}_{8}O_{11}$, $^{21}_{10}Ne_{11}$, $^{21}_{11}Na_{10}$, $^{23}_{11}Na_{12}$, $^{23}_{12}Mg_{11}$, and $^{25}_{11}Na_{14}$. The Nilsson model has been used with success regarding the interpretation of the static properties of ^{21}Ne, ^{21}Na, and ^{23}Na but only recently has there been sufficient experimental information upon which to base a detailed comparison of the dynamic-level properties of the Nilsson model. Howard, Allen, and Bromley (6) and more recently Poletti and Start (7) have shown that the Nilsson model successfully predicts both the phase and magnitude of the multipole mixing ratios involving γ-ray transitions among the three lowest-lying levels of ^{21}Ne, ^{21}Na, and ^{23}Na. The latter authors have also made Nilsson model predictions for the analogous transitions in ^{23}Mg, assuming that the spin sequence for the ground and first two excited states is identical to that in the mirror nucleus ^{23}Na. They remark that the predictions should be quite accurate and point out that it would be quite surprising if the phases of the mixing ratios were found to be incorrect.

The energy levels of ^{23}Mg (8) have been determined mainly by means of the $^{24}Mg(^{3}He, \alpha)^{23}Mg$ reaction. This nucleus is radioactive (9) and decays primarily to the ^{23}Na ground state. This decay is superallowed (log ft = 3.7) which determines the ground state spin and parity of ^{23}Mg as $J^{\pi} = 3/2^{+}$. Angular distributions of α-particle groups populating the ground and first-excited state lead to $J^{\pi} = (3/2,\ 5/2)^{+}$ for both states. (10)

In view of the lack of experimental information concerning the ^{23}Mg nucleus and the success in interpretating the static and dynamic properties of the low-lying states of the other "central" N or Z = 11 nuclei by means of the Nilsson model, it was clear that an angular-correlation study of this nucleus was needed. Of nine nuclear reactions which could populate levels in ^{23}Mg, only the ^{24}Mg(^{3}He, α)^{23}Mg reaction (Q_o = 4.048 MeV) was applicable using the Duke University 4-MeV Van de Graaff accelerator. The remaining reactions had large ($\leq$ -4 MeV) negative Q-values (with the exception of the ^{21}Ne(^{3}He, n)^{23}Mg reaction) and would have required a tandem accelerator or cyclotron to initiate them. The ^{24}Mg(^{3}He, α)^{23}Mg reaction, however, was well suited for a study of ^{23}Mg for several reasons. In 1965 Roberson, Tilley, and Weller (11) developed a ^{3}He ion source for the Duke University Van de Graaff accelerator which could provide up to 500 nA of doubly-ionized ^{3}He ions at energies of up to 8.2 MeV. Since the reaction Q-value of the ^{23}Mg 4.353-MeV tenth-excited state was only slightly negative (Q_{10} = -0.305 MeV), it was felt that most of the low-lying levels of ^{23}Mg could be populated with the available ^{3}He beam. The major advantage in using this reaction is that it is well suited to the angular-correlation method of axial symmetry.

Historically, the utilization of the symmetry of the reacting system in a nuclear reaction to simplify the theoretical analysis associated with an angular-correlation experiment was first pointed out by Biedenharn, Arfken, and Rose (12) in 1951. The method was first applied by Warburton

and Rose (13) in a γ - γ angular-correlation experiment. The method of axial symmetry as applied to particle-γ angular correlations has been attributed to J. Newton. (14) This whole method has been put in a more useful form by Litherland and Ferguson (15) and has been widely used.

Essentially, the particle-γ angular-correlation method is one of imposing constraints on the angular distribution of the de-excitation γ rays from an excited state formed in a nuclear reaction by detecting the reaction particles in an axially-symmetric detector positioned along the incident beam axis. These constraints depend on both the spin of the γ-ray emitting state and the multipole mixing ratio of the γ rays. The analysis of the γ-ray angular distributions can often lead to a unique set of these parameters. An important advantage of the method is that the analysis of the particle-γ angular correlations is independent of the reaction mechanism for the formation of the γ-ray emitting state. These remarks will be expanded in Chapter III.

A particle angular-distribution experiment was not considered for the present study as DWBA theory is not very reliable at the beam energies available in this laboratory. Such an experiment could, in principle, yield ℓ_n values and spectroscopic parameters which would be quite useful information.

B. The Present Experiment and Other Recent Work on ^{23}Mg.

An investigation of the ^{23}Mg nucleus using the particle-γ angular-correlation method of axial symmetry (referred to as Method II in Ref. 15) was begun in an effort to make rigorous spin assignments where possible or to limit rigorously the possible level spins, and to compare experimentally determined spins, decay modes, and mixing ratios with the predictions of the Nilsson model. In addition to elucidating the nuclear structure of ^{23}Mg, such a study could help to remove some ambiguities regarding experimental spin assignments in the mirror nucleus ^{23}Na and thereby lead to a greater understanding of the nuclear systems with N or Z = 11.

Approximately six months after this investigation was begun, work of a preliminary nature concerning the ^{23}Mg nucleus was reported by a number of groups. Joyce, Zurmuhle, and Fou,(16) using the ^{24}Mg(^{3}He, α) ^{23}Mg reaction, have made ℓ_n assignments to the angular distributions of α particles leading to several low-lying levels of ^{23}Mg. Ganguly et al. (17) and Kozub and Kashy (18, 19) have measured deuteron angular distributions from the ^{24}Mg(p, d)^{23}Mg reaction (Q_o = -14.328 MeV) and have assigned ℓ_n values to a number of levels in ^{23}Mg. Dubois and Earwaker (20) have performed an α-γ angular-correlation and α-particle angular-distribution experiment using the ^{24}Mg(^{3}He, $\alpha\gamma$)^{23}Mg reaction and report spin-parity assignments for the first three excited states of ^{23}Mg and limit the spins of three other levels to two possible values. A preliminary report on the

study of this same reaction at Duke University has been given. (21) Spin assignments and mixing ratios were given for the first two excited states and the isotropy of all of the γ rays from the decay of the third-excited state was indicated.

Work of a more definite nature has been recently published by Hay and Kean (22) who found eleven new levels in ^{23}Mg between 4.40 and 6.24 MeV excitation using the ^{24}Mg(^{3}He, α)^{23}Mg reaction. DaSilva et al. (23) have reported the results of their study of this same reaction. They make spin assignments for the first two excited states of ^{23}Mg and limit the spins of two higher states to two possible values. Quite recently, Dubois and Earwaker (24) have published the results of their study of ^{23}Mg.

It was realized that the work undertaken in this investigation would overlap the work of the various groups mentioned above and possibly of others due to the keen interest of nuclei in this region of the 2s-1d shell. However, it was felt that this independent study would be useful in that it could help to confirm or refute the work of other groups working simultaneously on ^{23}Mg and hopefully would provide additional information not determined by other groups.

In mid-1967 a large-volume Ge(Li) γ-ray detector was acquired by North Carolina State University. A coincidence measurement was performed utilizing the high intrinsic resolution of this detector to study the decay modes of ^{23}Mg. This information greatly complemented the angular-correlation measurements.

Chapter II

EXPERIMENTAL APPARATUS AND PROCEDURE

A. Angular-Correlation Measurements

1. General

The present investigation was carried out using the Duke University 4-MeV Van de Graaff accelerator equipped with a ^{3}He ion source. This source made it possible to obtain a doubly-ionized ^{3}He beam of good intensity with energies up to 8 MeV. The ^{3}He beam, containing both doubly-ionized and singly-ionized components, was accelerated and then magnetically analysed by a switching magnet. This magnet has beam ports which make it possible to control the accelerator with the $^3He^+$ beam while using the less intense $^3He^{++}$ beam for bombardment. The terminal potential was monitored using a precision ac digital voltmeter and was maintained to within ± 10 keV during all phases of this experiment.

After magnetic analysis, the $^3He^{++}$ beam passed through a set of remotely controlled slits which were located approximately 2 m from the switching magnet and were used to limit the beam intensity. Shielding

was provided around the exit of the slits to reduce extraneous radiation. The slits were followed by a magnetic-quadrupole lens and two beam deflectors which were utilized to guide the beam into the target chamber located approximately 5 m from the switching magnet. By optimizing the accelerator ion-source parameters and proper positioning of the lens and deflectors it was possible to focus the beam entirely through a 2.38-mm diameter collimator located approximately 30 cm from the center of the target chamber.

2. The Target Chamber

The angular-correlation chamber and associated collimation system are illustrated in Figure 1. The chamber itself was a 15.6-cm diameter brass cylinder with a 1.59-mm wall and a 9.53-mm bakelite top and bottom sealed to the cylinder by o-rings. The chamber was supported at each end by the beam pipe and could be rotated about the beam axis and also about a point defined by a ball joint positioned approximately 60 cm in front of the chamber. The top of the chamber contained a lucite window which allowed inspection of the target which was mounted on a 1.9-cm diameter, 1.59-mm thick stainless-steel ring. This ring was attached to a rod passing through the bottom of the chamber and could be rotated or pulled out of the path of the beam. The beam was collected in a Faraday cup located approximately 1.5 m from the target chamber and was measured using an Elcor Model A309B current integrator. (25) An oil diffusion

Figure 1. Top View of Angular-Correlation Chamber.

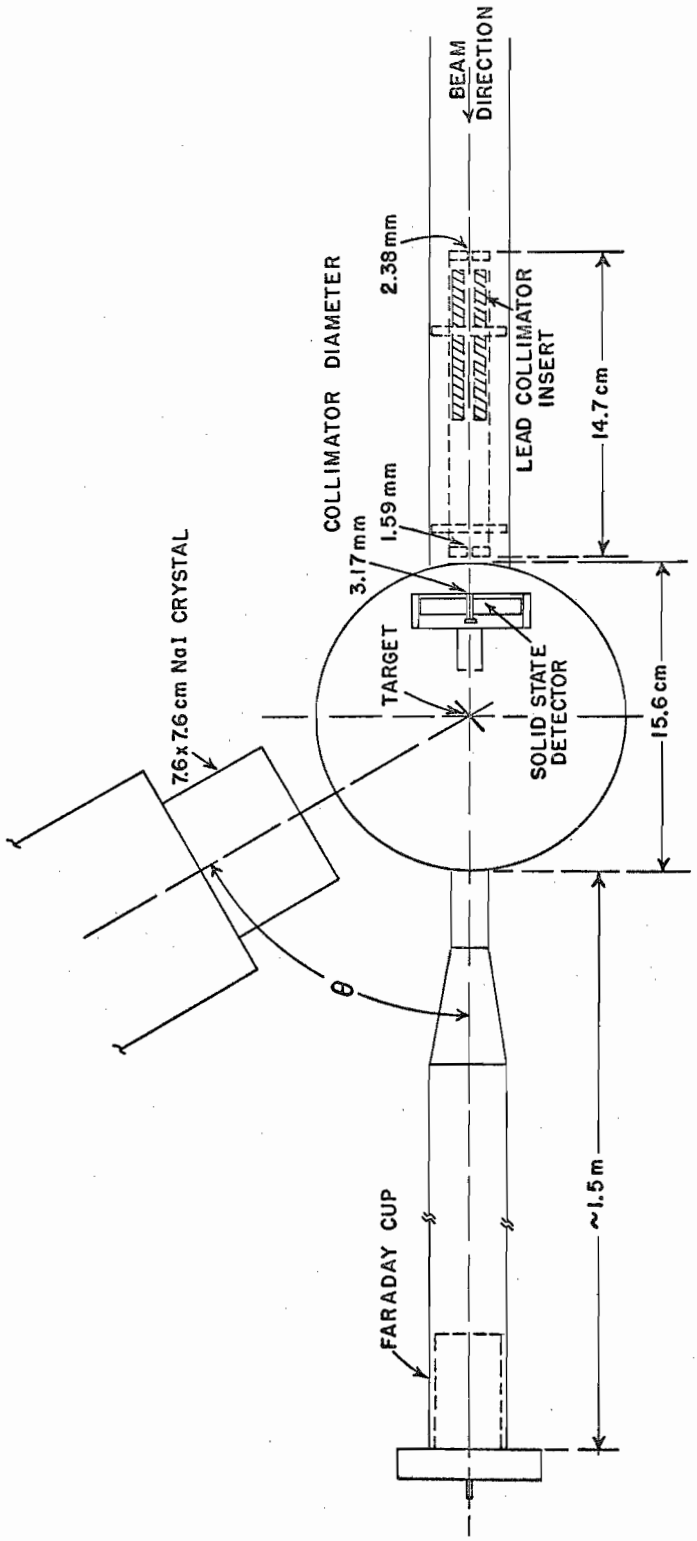

TOP VIEW OF CORRELATION CHAMBER

pump located between the Faraday cup and target chamber provided a vacuum of approximately 50 μtorr in the chamber.

The beam was initially collimated by a 2.38-mm diameter Ta collimator attached to a 14.7-cm long stainless-steel tube as shown in Figure 1. Additional collimation was provided by a 1.59-mm diameter Ta collimator attached to the other end of the tube. A 3.17-mm diameter stainless-steel insert, which was mounted in the solid-state detector holder, served as the anti-scattering collimator. Lead cylinders were placed in the tube to reduce the γ radiation caused by the beam striking the first collimator.

The charged-particle detector was mounted in a lucite holder with an attached snout which was designed to prevent radiation scattered by the chamber walls from striking the sensitive area of the detector. A small lip on the 3.17-mm diameter insert served to shield the rough inner edge of the detector from the back-scattered radiation.

3. Target Preparation

The ^{24}Mg targets were prepared by evaporating MgO enriched to 99.96% ^{24}Mg (26) onto plain 3 x 1-inch glass slides or onto glass slides which supported a thin carbon backing. The oxide was partially reduced by adding Ta powder to the MgO prior to evaporation from a Ta boat. The targets evaporated onto the carbon backings were readily floated off the slides in water and mounted on the stainless-steel rings. The self-supporting targets, however, could only be removed from the slides after

evaporating the MgO-Ta mixture at a rapid rate. This technique presumably caused a water-soluble oxide layer to be deposited onto the glass slides before the magnesium metal began to evaporate. It was then possible to float the shiny, metallic films from the slides in a water bath and mount them on the target rings. It has recently come to the attention of the author that BaI_2 and CsI are good release agents in removing evaporated isotopes from substrates. The slides can be uniformly coated with these water-soluble compounds by vacuum evaporation before evaporating the isotope. The targets can then, presumably, be readily floated from the slides in a water bath.

Both self-supporting and carbon-backed targets were used during the experiment. The latter targets, however, were easier to produce and were less likely to break under long bombardment and high beam currents. The thickness of the ^{24}Mg targets was of the order of 75 $\mu gm/cm^2$ and that of the carbon backings approximately 15 $\mu gm/cm^2$. The only criteria used in selecting a target thickness were that the resolution be adequate to resolve the α groups of interest and the thickness be sufficient to yield a reasonable coincidence counting rate.

4. Reaction Product Detection

a. Alpha-Particle Detector. The charged-particle spectrum from the target was detected by a silicon surface barrier detector mounted at 180° to the ^3He beam and 4 cm from the target. This detector, supplied by ORTEC (27), was fabricated from 950 ohm-cm silicon, was of 100 mm^2

area, and contained a 4-mm diameter hole through which the ^{3}He beam passed. The detector subtended a solid angle of approximately 0.06 steradians at the center of the target. The inner and outer edges of the sensitive area subtended angles at the target center of 173° and 177°, respectively. The counter could stop approximately 14-MeV α particles and approximately 3.5-MeV protons at a depletion depth of 100 μ. The use of a low-resistivity counter was necessary to insure that the pulses from the detector would be of sufficiently short rise time to trigger the time pickoff unit which furnished the timing signals for the coincidence measurements. The use of a thin counter also insured that protons from the (^{3}He,p) reaction would make a negligible contribution to the charged-particle spectrum.

b. Gamma-Ray Detector. The γ-ray detectors were cylindrical Na(Tl) crystals furnished by Harshaw. (28) The initial phase of this experiment was performed using a 5.1 x 5.1-cm crystal. Later a 7.6 x 7.6-cm and a 10.2 x 12.7-cm crystal were employed. The larger crystal was used to improve the statistics of the weak ground-state transition of the ^{23}Mg second-excited state, but the poor resolution of this crystal rendered the results questionable. The 7.6 x 7.6-cm crystal was found to possess the best resolution and efficiency for detecting the higher-energy γ rays encountered in this study. The faces of the 5.1 x 5.1-cm and 7.6 x 7.6-cm crystals were positioned 8.9 cm and 11.4 cm, respectively, from the target. Each crystal had a resolution of approximately 10%

FWHM for a 0.51-Mev γ ray. The 5.1 x 5.1-cm crystal was mounted on an RCA 6810-A photomultiplier tube (29) while the 7.6 x 7.6-cm crystal was used with an Amperex 58-AVP photomultiplier tube. (30) Both tubes were enclosed in μ-metal shields to minimize effects of external magnetic fields on the gain of the tubes. Optical coupling between the crystals and tubes was provided by Dow Corning 200 fluid (viscosity = 10^6 centistokes). (31)

The γ-ray detector was mounted on a trolley which rotated about a vertical axis through the center of the target chamber. The detector angular settings were indicated on a 360° calibrated table mounted directly beneath the target chamber. The angular readings were made with an error not greater than 0.5°.

5. Electronics

Figure 2 is a block diagram of the coincidence circuit used to perform a two-parameter analysis of the α-γ coincidences from the $^{24}Mg(^3He, \alpha\gamma)^{23}Mg$ reaction. This circuit, in conjunction with an on-line computer, made it possible to obtain, simultaneously, angular-correlation data on up to ten excited states of ^{23}Mg.

The Amperex 58-AVP photomultiplier tube and Model PA58 base was used for the majority of the angular-correlation measurements. This tube is a 14-stage, very fast, high-gain photomultiplier with a Cs-Sb, semi-transparent, curved cathode of approximately 12.7-cm diameter. The anode pulse has a rise time of 2 ns which makes the tube ideally suited for use with fast coincidence circuitry. It was observed with initial use of

Figure 2. Block Diagram of Electronics Used for the Angular-Correlation Measurements.

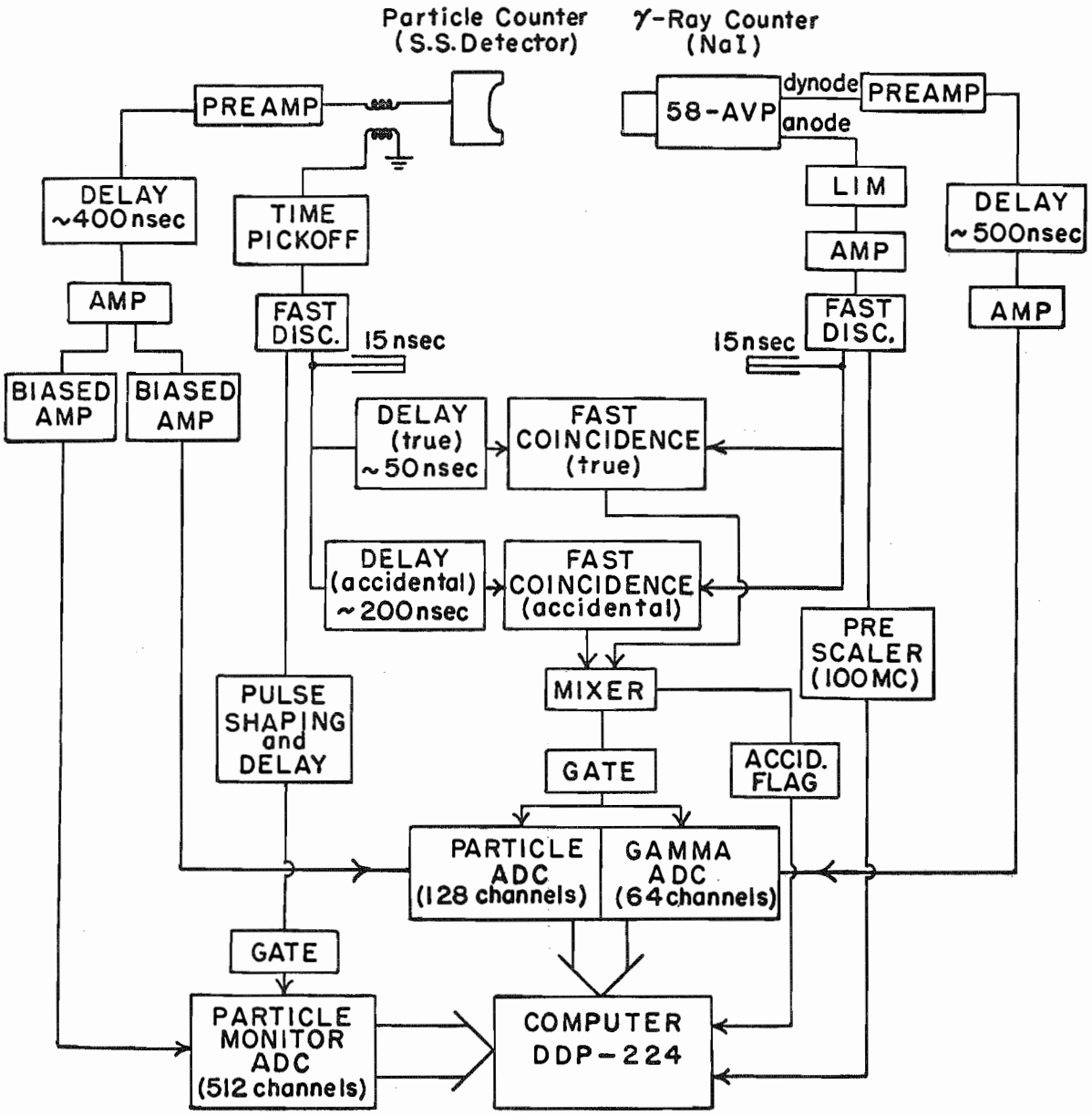

BLOCK DIAGRAM OF ELECTRONICS

the tube base that there were rather large pulse-height changes due to high counting rates in the output from the base. This problem was corrected by decreasing the total resistance of the resistor bank in order to increase the bleeder current. This modification acted to stabilize the voltage across each dynode which led to greater gain stability in the tube. Severe voltage fluctuations were also observed during initial use of the tube. This problem was corrected by fixing the conducting layer on the wall of the tube at the same negative potential as applied to the cathode. The circuit diagram showing these modifications is given in Reference 32.

Linear signals, used for energy analysis, were taken from the 14-th dynode of the photomultiplier and amplified by an ORTEC Model 113 preamplifier. These signals were then delayed approximately 500 ns, amplified by a Hamner Model N-301 linear amplifier (33), and used as one input to a TMC 1024-channel dual analog-to-digital converter (ADC). (34)

Fast γ-ray pulses were taken directly from the anode of the photomultiplier and driven directly to the accelerator console area through 50-ohm cable chosen for impedance matching. It was necessary to limit these pulses to protect the fast coincidence circuitry from excessively high voltages. The limiter circuit is given in Reference 35. The limited pulses were amplified by a Chronetics Model 106 pulse amplifier (36) having a fixed gain of ten and a rise time of 2 ns. These amplified pulses were then fed into a Chronetics Model 101 dual discriminator with a fixed 1.5 μs output pulse width, a width long enough to prevent double pulsing.

Linear signals from the annular detector were amplified by an ORTEC Model 109 charge-sensitive preamplifier. These signals were delayed approximately 400 ns and amplified by an ORTEC Model 410 pulse-shaping amplifier. This amplifier provides simultaneous unipolar (singly differentiated) and bipolar (doubly differentiated) outputs with RC or delay-line shaping. The bipolar signal was used as the input for both an ORTEC Model 408 and a RIDL Model 30-21 biased amplifier. (37) These amplifiers allowed only those portions of the spectrum which were of interest to be analysed. The unipolar signal was fed into an oscilloscope and was used as a visual monitor of pulses from the annular detector. The output of the ORTEC biased amplifier served as the input to the second half of the TMC dual ADC.

The time of arrival of particles detected by the annular detector was derived from an ORTEC Model 260 time pickoff used in series between the detector and the charge-sensitive preamplifier. A toroidal transformer in this unit inductively taps the leading edge of the detector signal without appreciably affecting the linear signal which is fed to the preamplifier. These timing signals, from the secondary of the transformer, then actuate a fast amplifier and tunnel diode discriminator. When used with the low-resistivity detector, the time pickoff proved to be an efficient source of timing signals. The fast signals were driven through 50-ohm cable to a Chronetics Model 114 fast discriminator.

The logic pulses from the fast-α and fast-γ discriminators

were clipped to a width of 20 ns and fed into a Chronetics Model 107 two-fold coincidence circuit which furnished the fast coincidence pulses. Due to the relatively slow rise time of pulses from the NaI crystal (typically 200 ns) and electron transit time in the photomultiplier tube, it was necessary to delay the fast-α signal 40 ns relative to the fast-γ signal in order for the two pulses to overlap in time. Accidental coincidences were determined by routing the clipped-α and -γ logic signals into the second half of the Chronetics fast coincidence circuit but with the fast-α signal delayed approximately 200 ns relative to the fast-γ signal. The overall time resolution of the fast coincidence circuitry was approximately 40 ns.

The output pulses from the true-plus-accidental (total) and accidental coincidence circuits were fed into a mixer circuit which generated a gate pulse for both the particle ADC and the γ ADC. This circuit also provided a signal by which accidental coincidences stored in the computer could be distinguished from total coincidences.

A Computer Control Company Model DDP-224 computer (38) was programmed as a 256 x 64-channel, two-parameter analyser with 64 channels assigned to the γ-ray spectrum and 256 channels assigned to the α-particle spectrum. For each α particle group stored along the 256-channel axis, the associated γ-ray coincidence spectrum (total and accidental) was stored along the 64-channel axis. The total and accidental coincidences were recorded in binary form on magnetic tape and later read back into the computer for data analysis. Only 128 channels of the 256-channel axis

could be read back at one time as the computer had only an 8 K memory.

The effect of dead time in the γ-ray discriminators was determined by counting the number of γ rays detected during each angular measurement. This was accomplished by scaling the counting rate down by a factor of 10^5 using a Chronetics Model 109 100 mc prescaler in series with a modified RIDL scaler. The number of γ rays so detected was then stored in the computer along with the coincidence data. Using the measured 2.5 μs dead time for the γ-ray circuitry, a dead time correction was calculated. This correction was essentially insignificant as care was taken to maintain a constant beam current for each angular measurement.

The normalization of the α-γ correlation data was based on a 512-channel α-particle monitor spectrum recorded in a way which could account for changes in the bias level of the time pickoff unit. Pulses from the annular counter which were subsequently amplified by the RIDL biased amplifier were fed into a Victoreen 2048-channel ADC (39) which was gated by the time pickoff signal generated by a fast discriminator. In this manner changes in the bias level of the time pickoff, which affected the α-γ coincidence rate, could be accounted for by normalizing the angular measurements for a particular α-particle group to the number of counts recorded for that same group in the monitor spectrum. The monitor spectra were recorded in binary form on magnetic tape for later analysis. These spectra and also the two-dimensional data were displayed on an oscilloscope as the data were accumulated and provided a visual monitor of the experiment.

6. Procedure

a. Alignment. The target chamber was initially aligned by adjusting its orientation so that the ^{3}He beam impinged upon the center of a quartz crystal positioned near the target chamber exit. The magnetic lens and deflectors were not used during this state of the alignment. The annular counter and target-ring support were then aligned using a carefully made brass rod designed to pass through an insert located at the target chamber exit, the target ring, the annular counter, and finally the 1.59 mm diameter collimator positioned at the target chamber entrance. This alignment was verified by bombardment of a carbon target with the ^{3}He beam. The 1.59-mm diameter beam spot was found to be centered on the target.

The center of the calibrated table upon which the γ-ray detector rotated was positioned under the center of the target chamber using a plumb line attached to the target rod. Plumb lines suspended from both sides of the beam pipe were also used to position the 180° position of the calibrated table directly under the center of the beam pipe. The γ-ray detector was centered relative to the target by aligning the central axis of the cylindrical crystal and attached photomultiplier with the center of the target.

The overall alignment of the system was verified by measuring the ^{12}C(d, p$_1\gamma$)^{13}C angular correlation which is known to be isotropic as the ^{13}C 3.09-MeV first-excited state has $J^{\pi} = 1/2^{-}$. (40) This correlation was found to be isotropic to within 2%.

b. Excitation. Ten excited states in ^{23}Mg have been identified up to 4.353 MeV, primarily by means of the ^{24}Mg(^{3}He, α) ^{23}Mg reaction. (8) Recently many more levels have been identified at higher energies. (22, 24) The work in this study, however, is limited to the first ten excited states. Of these levels, the states at 0.451, 2.048, 2.356, and 4.353 MeV are well separated from nearby levels and consequently posed no special resolution problems. Two close-lying levels exist at 2.712 and 2.768 MeV, the latter level separated by 136 keV from the sixth-excited state at 2.904 MeV. Another set of close-lying levels exists at 3.792 and 3.856 MeV with the latter level separated by 112 keV from the ninth-excited state at 3.968 MeV. While it was impossible to fully resolve these two sets of three close-lying states an attempt was made to find bombarding energies at which some of these states would be preferentially excited. This was accomplished by evaporating a thin film of ^{24}Mg onto a thin carbon backing and observing the α-particle yield in the annular counter as a function of ^{3}He bombarding energy. The levels populated were then identified with the aid of the reaction kinematics. Bombarding energies of 6.37 and 8.00 MeV were chosen as the optimum energies at which to perform the angular-correlation measurements. The α-particle spectra recorded at these two energies are shown in Figure 3. At 6.37 MeV the first-, third-, sixth-, and tenth-excited states were populated with approximately the same cross section. The second-excited state was only weakly excited. The 2.712, 2.768-MeV doublet was weakly excited relative to the nearby sixth-excited state and

Figure 3. Alpha-Particle Spectra from the $^{24}Mg(^{3}He, \alpha)^{23}Mg$ Reaction Recorded in the Annular Detector at ^{3}He Bombarding Energies of 6.37 and 8.00 MeV. The α-particle groups are labeled by the state in ^{23}Mg to which they lead. The arrows indicate the expected position of the corresponding α-particle groups as determined from the reaction kinematics.

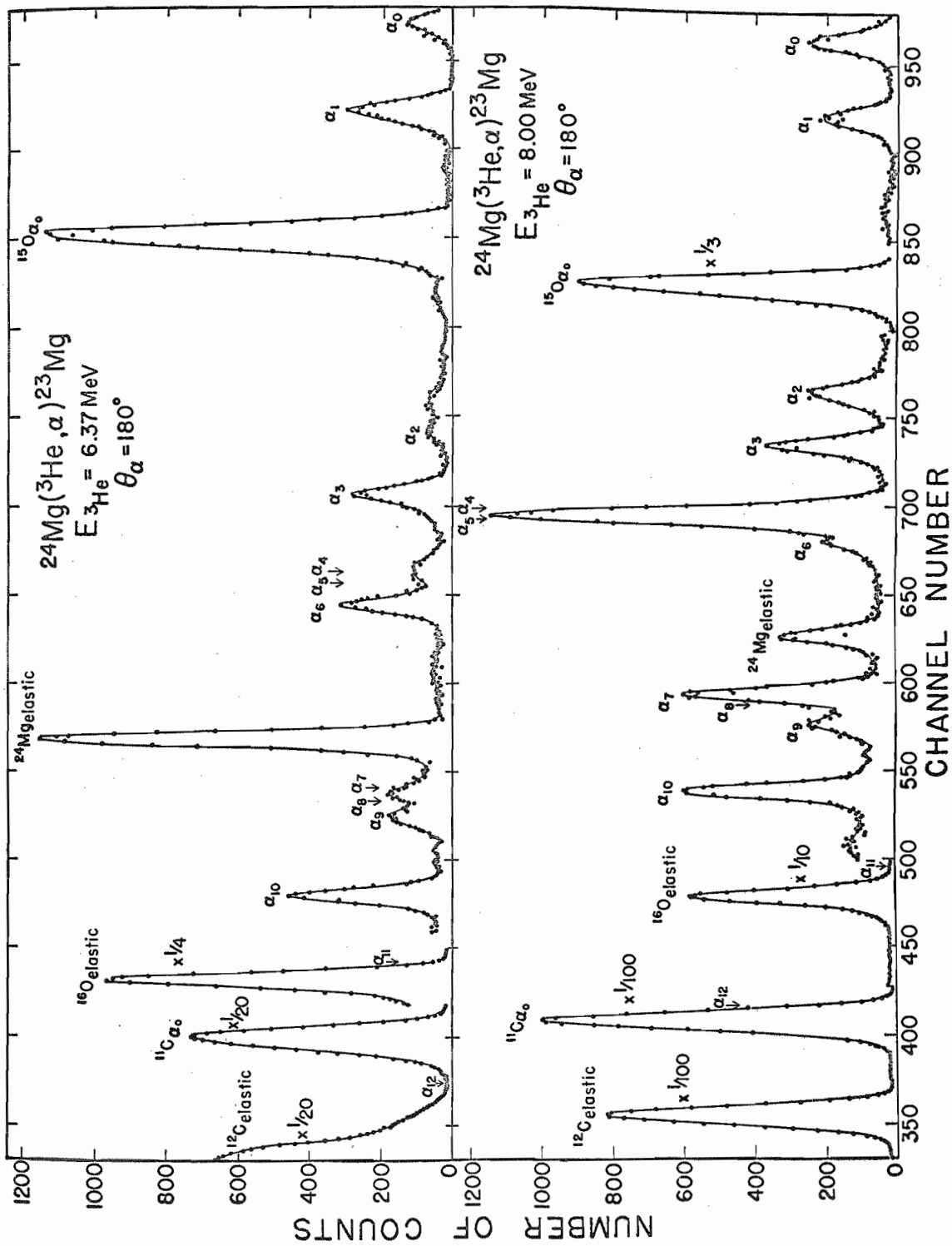
24Mg(3He,α)23Mg
E3He = 6.37 MeV
θα = 180°
24Mg(3He,α)23Mg
E3He = 8.00 MeV
θα = 180°
NUMBER OF COUNTS
CHANNEL NUMBER
24Mgelastic
16Oelastic
11Cα0
12Celastic
15Oα0
α0
α1
α2
α3
α4
α5
α6
α7
α8
α9
α10
α11
α12
x1/4
x1/20
x1/100
x1/10
x1/3

the ninth-excited state at 3.968 MeV appeared to be populated more than the 3.792-, 3.856-MeV doublet. At a ^{3}He energy of 8.00 MeV the second-excited state was reasonably well excited so that a correlation measurement was feasible. The 2.712-, 2.768-MeV doublet was very strongly populated relative to the 2.904-MeV level. The thin-target yield also indicated that the 3.792-MeV seventh-excited state was fed more strongly than the levels at 3.856 and 3.968 MeV. It thus appeared that for these two bombarding energies information could be obtained on the decay modes of nine excited states of ^{23}Mg. It was doubtful that any information could be obtained concerning the weakly excited 3.856-MeV level.

Yield curves of α particles detected at 180° to the beam axis and leading to the ^{23}Mg ground state and first three excited states are shown in Figure 4. The rather large fluctuations in the yield suggest that there is considerable compound nucleus formation in the beam-energy region (6.0 - 8.2 MeV) studied here. This same behavior was observed by Dubois and Earwaker (24) for the ^{3}He energy range 8-11 MeV with the α particles detected at 10° relative to the beam axis. The small relative cross section for exciting the 2.048-MeV level suggests that the spin of this level differs from that for the ground state and first- and third-excited states. The spins of these states, to be discussed later, are given in Figure 4 for comparison.

c. Delays. Coincidences between the fast-α and fast-γ logic signals were established by delaying the α signal 40 ns relative to the γ

Figure 4. $^{24}Mg(^{3}He, a)\,^{23}Mg$ Excitation Spectra Recorded in the Annular Detector for the ^{3}He Energy Range 6.0-8.2 MeV.

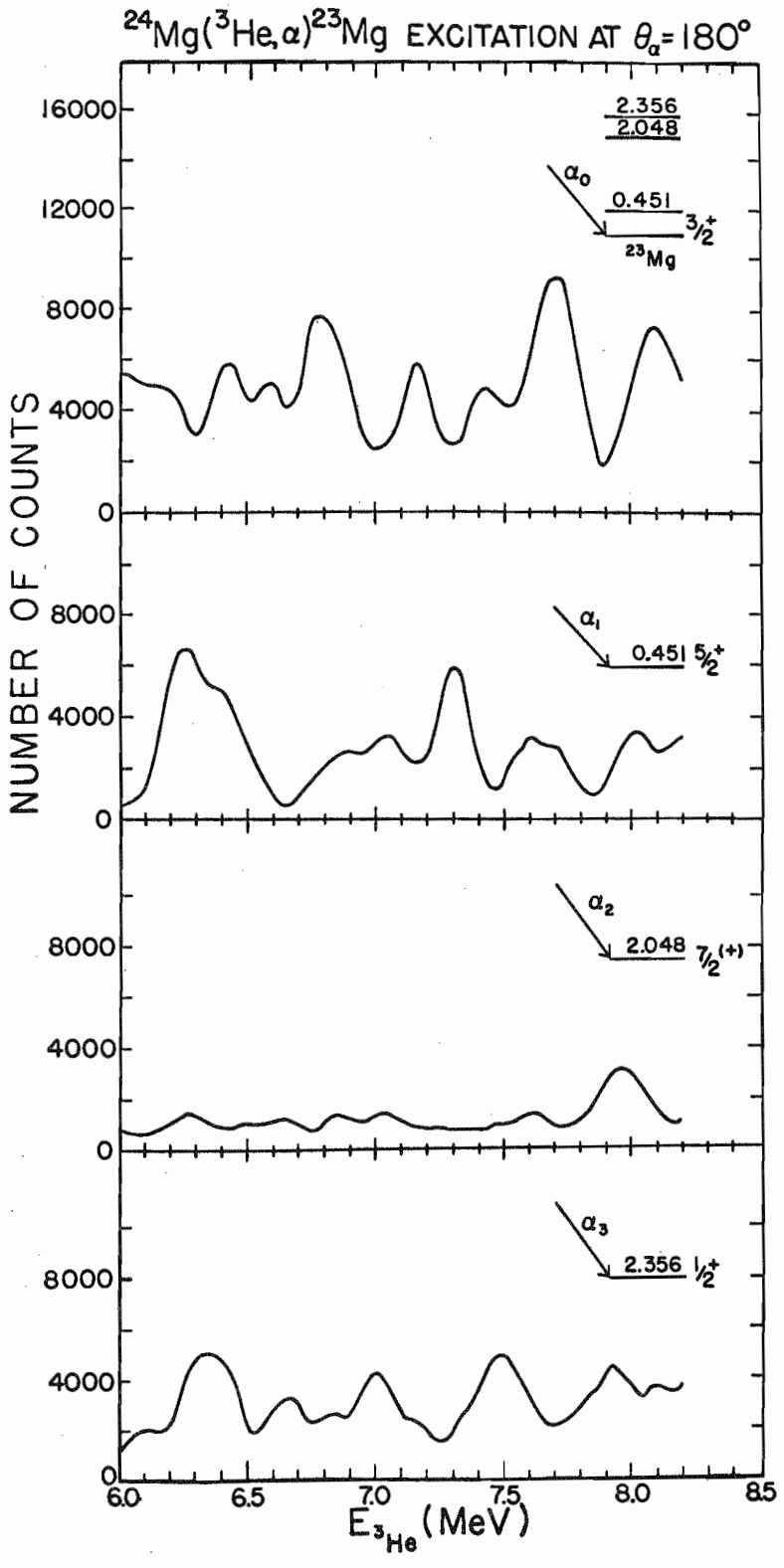
$^{24}Mg(^{3}He,\alpha)^{23}Mg$ EXCITATION AT $\theta_\alpha = 180°$
NUMBER OF COUNTS
16000
12000
8000
4000
0
2.356
2.048
α_0
0.451
$3/2^+$
^{23}Mg
α_1
0.451 $5/2^+$
α_2
2.048 $7/2^{(+)}$
α_3
2.356 $1/2^+$
6.0
6.5
7.0
7.5
8.0
8.5
$E_{^3He}$ (MeV)

signal. This delay was determined using a Chronetics Model 105 time-to-pulse-height (TPH) converter. This device is designed to convert the time overlap of two standardized pulses to a pulse whose height is proportional to the time overlap between the two pulses. A pulse from the fast-α discriminator, clipped to a pulse width of 100 ns, was split and fed into the two inputs of the converter. The output was then fed into a TMC 400-channel analyser for pulse height analysis. The peak channel so determined corresponded to that expected for two perfectly overlapping pulses. The fast-α and fast-γ logic signals, both clipped to 100 ns pulse width, were then routed into the TPH converter. Delay was introduced between the two pulses until the coincidence peak fell in the channel of the analyser expected for perfect overlap. As previously mentioned, the accidental coincidences were established by delaying the fast-α signal 200 ns relative to the fast-signal.

d. Timing Measurements. Initial use of the time pickoff unit indicated that the device was extremely sensitive to noise pulses which existed in the laboratory. There was also a tendency of the discriminator level of the tunnel diode to drift downwards. Both of these effects tended to cause oscillation of the tunnel diode discriminator. A circuit was devised which prevented data from being stored by the computer while the discriminator was oscillating. The noise pulses were considerably reduced by surrounding the pickoff unit, the charge-sensitive preamplifier, and the target chamber with brass screen.

An upwards drift of the discriminator level was also observed occasionally during the runs. This effect was of little concern since it caused only a decreased efficiency in the time pickoff which would be reflected in the monitor spectra to which the data were normalized. The question arose, however, as to the effect of these drifts, in the time pickoff triggering level, on the resolving time of the coincidence circuitry. To resolve this question a two-parameter analysis was performed of the TPH-converter signals as a function of α-particle energy. Linear, amplified pulses from the annular counter and logic pulses from the converter were fed into separate sections of the TMC dual ADC, both of which were gated by the fast coincidence pulses. Several two-dimensional spectra were recorded in this manner for a wide range of time pickoff bias levels. These measurements revealed that the time resolution of the coincidence circuit was not a function of the pickoff bias level.

A similar measurement was performed for the converter timing signals as a function of γ-ray energy. It was observed that a somewhat longer resolving time was required to record α-γ coincidences for γ rays with energies less than approximately 1 MeV than that required at higher energies. This effect is a result of the long rise time of pulses from the NaI crystal and is one of the limitations of leading-edge timing. However, this measurement revealed that a resolving time of $2\tau = 40$ ns was sufficient to record coincidences for γ rays with energies as low as approximately 400 keV.

e. Angular Measurements. The angular-correlation measurements consisted in determining the intensity of α-γ coincidences as a function of the direction of emission of the γ rays relative to the beam axis with the α-particle detector fixed at 180° relative to the beam. The measurements were performed at five angles of the γ-ray counter between 26° and 90°. These angles were chosen in a random order to reduce the effect of possible drifts in the system. The measurements were also performed on the opposite side of the chamber to compensate for any asymmetries associated with rotation of the target, fluctuations in the beam, or in positioning of the γ-ray counter. At least two or more of the angular measurements were repeated on each side of the target chamber. The target was oriented at 30° to the beam axis and faced the NaI detector. The target was rotated when the NaI detector was moved to the opposite side of the chamber. This avoided any absorption of low-energy γ rays by the stainless-steel target ring. Each angular measurement lasted for five hours. Beam currents of 100 nA were employed. The measurements performed at a ^{3}He energy of 6.37 MeV were repeated once and those at 8.05 MeV were repeated twice.

f. Extraction of the Angular Correlations. The total and accidental coincidence spectra obtained for each angular measurement were recorded on magnetic tape and later read back into the computer for analysis. Figure 5 shows the x- and y-axis projections of a typical two-dimensional spectrum obtained at $\theta = 90^{\circ}$ and at a ^{3}He energy of 8.05 MeV.

Figure 5. X- and Y- Axis Projections of 2-Dimensional Coincidence Spectrum from the $^{24}Mg(^{3}He, \alpha\gamma)^{23}Mg$ Reaction. The x-axis projections, labeled A, B, and C, are the γ rays coincident with selected portions of the α-particle spectrum shown on the left and denoted by A, B, and C. The α-particle groups are labeled by the energy in MeV of the level in ^{23}Mg to which they lead. The γ rays are labeled by transition energies given in MeV. The ^{23}Mg level schemes, appropriate to the selected regions A, B, and C of the particle spectrum, are also shown. These spectra are the result of a single measurement made at $\theta = 90^{\circ}$ and at a ^{3}He energy of 8.05 MeV. Accidental coincidences have been subtracted.

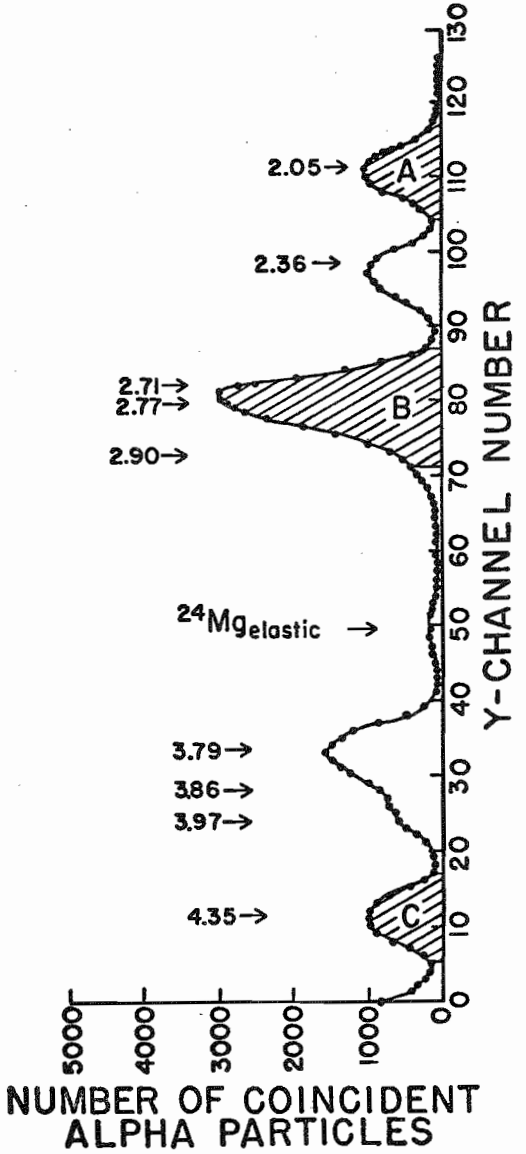
2.05→
A
2.36→
2.71→
2.77→
B
2.90→
24Mgelastic →
3.79→
3.86→
3.97→
4.35→
C
Y-CHANNEL NUMBER
NUMBER OF COINCIDENT ALPHA PARTICLES

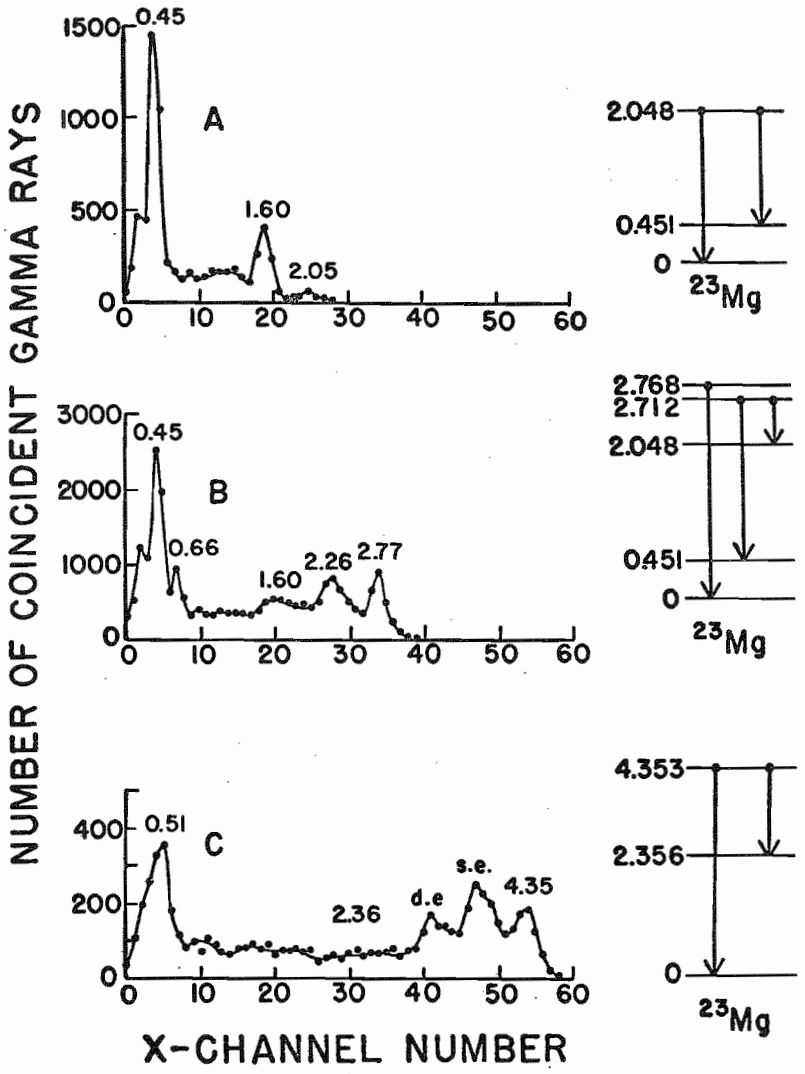
NUMBER OF COINCIDENT GAMMA RAYS
0.45
A
1.60
2.05
0.66
B
2.26
2.77
0.51
C
s.e.
d.e
4.35
2.36
X-CHANNEL NUMBER
2.048
0.451
23Mg
2.768
2.712
4.353
2.356

The α-particle spectrum, displayed on the y axis, was obtained by performing a block sum of the entire 64 x 128-channel spectrum and projecting the result onto the y axis. The coincident γ-ray spectrum associated with a particular α-particle group was obtained by summing the region of the y axis corresponding to that particle group and projecting the sum onto the x axis. The accidental coincidence spectrum was subtracted by reading the accidental coincidence spectrum for the same run into the computer and performing the block sum with the same y-axis coordinates. The resulting x-axis projection was then subtracted from the initial projection resulting in the true coincidence spectra shown in Figure 5. Summed γ-ray spectra, which were used to determine branching ratios, were obtained by accumulating the γ-ray spectra recorded at all angles for a particular α-particle group. The corresponding accidental coincidence spectra were subtracted.

The individual γ-ray spectra corresponding to each particle group were plotted, and in cases where gain shifts existed on the γ-ray axis the energy calibration for each spectrum was used to sum a particular energy interval for each γ ray. In some cases the γ-ray spectra were each normalized to the same gain before summing. These sums were then normalized using the monitor spectra discussed previously. Gamma-ray spectral shapes were used where necessary to extract the angular correlations. The procedure used to analyse each particular correlation will be discussed in more detail in Chapter III.

B. Ge(Li) Detector Coincidence Measurements

1. General

High resolution γ-ray coincidence measurements were performed with the Ge(Li) detector to help determine the decay modes of the low-lying levels of ^{23}Mg and particularly the 2.712-, 2.768-MeV doublet. These measurements also led to a confirmation of the energies of many of the ^{23}Mg levels.

2. The Ge(Li) Detector

The Ge detector was an ORTEC lithium-drifted germanium diode in the form of a right circular cylinder with both ends open. The total active volume was 20.6 cc. The measured total resolution for 1.33-MeV γ rays using an ORTEC Model 118A preamplifier and Model 410 pulse-shaping amplifier (2 μs time constant, single RC shaped) was 4.1 keV FWHM. The detector was mounted on an ORTEC Model 81 right angle cryostat which contained liquid nitrogen. The detector-cryostat assembly was furnished with a Model 118A preamplifier mounted directly to the cryostat to minimize the preamplifier input capacitance.

3. Target Chamber

The target chamber was a nickel-plated copper cylinder 7.63-cm in diameter with 3.17-mm thick walls. Aluminum plates 9.53-mm thick were sealed to the top and bottom of the chamber by o-rings. Targets

were mounted in this chamber as in the correlation chamber. The annular counter was mounted at 180° to the beam axis and was supported by a holder similar to that used in the correlation chamber. The Ge(Li) detector could be positioned flush with the wall of the chamber. Beam collimation was provided by two 1.59-mm diameter Ta collimators and a 3.17-mm diameter anti-scattering collimator inserted in the annular counter support. The beam was collected in a Faraday cup located approximately 1.5 m from the chamber.

4. Electronics

The electronic circuit used to observe coincidences between α particles detected in the annular counter and γ rays detected with the Ge detector was similar to that used for the angular-correlation measurements. The main difference between the two circuits was the manner in which the fast signals were obtained from the Ge detector. A block diagram of the electronics associated with this detector is illustrated in Figure 6.

Following a suggestion by ORTEC, the fast-γ signal was obtained from an ORTEC time pickoff inserted into the circuit as shown in the figure. By placing the pickoff between the preamplifier and pulse-shaping amplifier a low triggering threshold may be achieved with little energy resolution degradation and with the time resolution affected only slightly by the preamplifier rise time. The plug-in inductor (L3) in the ORTEC Model 260 time pickoff unit was changed from 0.56 μh to 5.6 μh

Figure 6. Block Diagram of Electronics Associated with the Ge(Li) Detector.

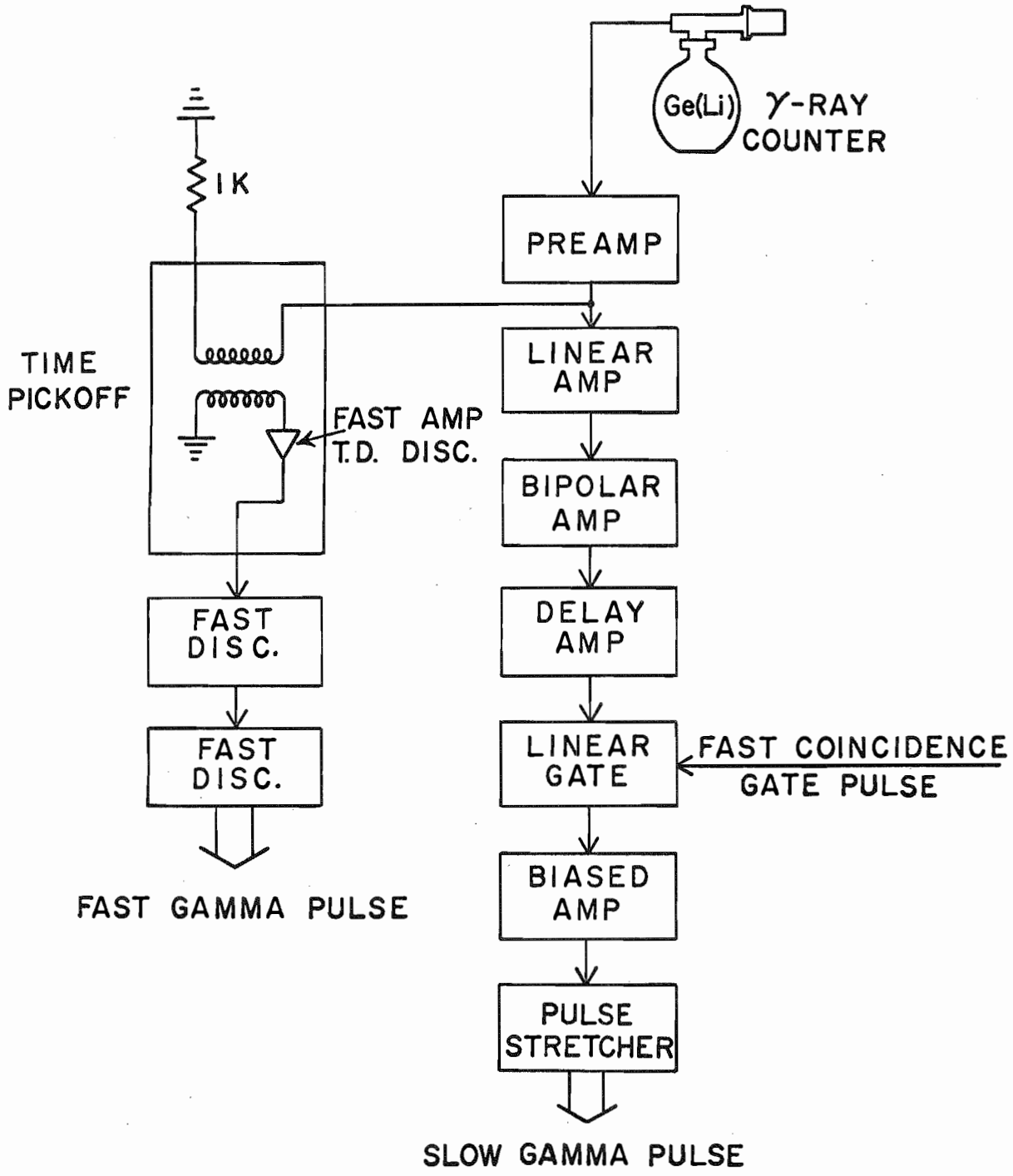
Ge(Li)
γ-RAY COUNTER
1K
PREAMP
TIME PICKOFF
LINEAR AMP
FAST AMP T.D. DISC.
BIPOLAR AMP
FAST DISC.
DELAY AMP
FAST DISC.
LINEAR GATE
FAST COINCIDENCE GATE PULSE
BIASED AMP
PULSE STRETCHER
FAST GAMMA PULSE
SLOW GAMMA PULSE

to prevent multiple trigger from the wide input signal. The fast-γ pulses were fed through two Chronetics Model 101 discriminators and then into a Chronetics Model 107 coincidence unit.

Pulses from the ORTEC Model 118A preamplifier, used for energy analysis, were amplified by the linear amplifier stage of an ORTEC Model 220 linear pulse analysis system and then by the bipolar stage. The bipolar pulse permits a much higher counting rate with less baseline distortion than would be possible with a unipolar signal. The first and second differentiation and integration time constants employed were each 1 μs. Signals from the bipolar amplifier were delayed 1.4 μs by the delay amplifier and fed into the linear gate which was gated with the fast coincidence signal. Gating the linear gate with this low counting rate signal reduced the number of pulses being fed to the γ-ray ADC and led to better energy resolution. In addition, the linear gate contained a dc baseline restoration network without which good energy resolution could not have been achieved. The linear gate pulses were fed into a biased amplifier followed by a pulse stretcher. The pulse stretcher stretches the peak voltage of the input signal, thereby reducing the bandwidth requirements of the ADC which in turn leads to improved linearity. Finally, the stretched pulses served as the input for the 2048-channel Victoreen ADC.

For these measurements the TPH converter spectrum was stored along with the α-γ coincidence spectrum so that the computer served as a three-parameter analyser. This procedure was necessary in order to

record the low-energy γ rays. A two-dimensional spectrum of the TPH converter signals versus γ-ray energy revealed that a much longer resolving time was required to detect α-γ coincidences for γ rays with energies below approximately 1 MeV than needed to detect higher energy ones. As with the NaI crystal, this effect is due to the long rise time of low-energy pulses from the Ge detector. In order to record γ rays with energies in the range 0.4 to 4.5 MeV a resolving time of approximately 100 ns would have been required. This would cause an inordinate number of accidental coincidences in the spectrum, masking the true coincidence events. However, by storing the TPH converter spectrum along with the coincidence spectrum smaller time intervals, e.g. 15 ns, could be chosen for a particular γ ray of interest. In this way a greatly reduced accidental/true ratio was obtained. Using three-parameter analysis the coincident γ rays could be labeled with the α-particle coordinates to which they corresponded and also with their time coordinates. This method of analysis clearly provides much more information than with the two-parameter analysis used for the correlation measurements.

The fast-α and fast-γ signals were both clipped to a pulse width of 100 ns and fed into the TPH converter after delaying the α signal 31 ns relative to the γ signal. The timing signals from the converter were amplified and fed into one side of the TMC ADC. The linear-α signals were routed into the other half of the ADC and the linear-γ signals were fed into the Victoreen ADC. Each ADC was gated by the fast coincidence gate pulse.

The data storage program provided 256 channels for the TPH axis, 1024 channels for the α-energy axis, and 2048 channels for the γ-energy axis. The TPH signals were delayed relative to the linear-γ signals so that the peak in the TPH spectrum fell approximately in the middle of the axis. This allowed the full time interval on the TPH axis to be seen.

The target chamber and annular detector were aligned so that the beam was centered on a carbon-backed ^{24}Mg target. The Ge detector was placed flush with the wall of the chamber and at 90° to the beam axis. The coincidence measurement was performed at a ^{3}He energy of 8.00 MeV. Each measurement lasted 5 hours after which the data were recorded on magnetic tape. A total of 150 hours of data were taken. There were no significant gain changes during this time on either the α- or γ-energy axis. Energy calibration spectra were recorded at frequent intervals using a RdTh (ThC") source. This source emitted γ rays with energies of 2.61425 ± 0.00050 MeV (photopeak) (41), 1.59237 MeV (double escape peak), and 0.51094 ± 0.00007 MeV (annihilation radiation). (42) These γ rays were used for the calibration. The γ-ray energy axis had the range of approximately 300 keV to 4.5 MeV with an energy dispersion of 2.070 keV/channel. The resolution for a 1.751-MeV γ ray was 19 keV FWHM.

5. Reduction of the Data

The first step in analysing the three-dimensional data was to read several runs into the computer to determine the coordinates of the

α-particle groups. The 2048-channel γ-ray axis was then divided, arbitrarily, into three regions: channels 37-400, 400-800, and 800-2048. The TPH spectra for several runs for γ rays in the channel range 800-2048 and for a particular set of particle coordinates were read into the computer. The peak observed then defined the time coordinates for this particular γ-ray energy interval. Each of the five hour runs was then searched for the γ rays with these particle and time coordinates. The resulting γ-ray spectra were summed. This procedure was followed for the γ-ray channels 400-800 and 37-400. The three summed spectra resulted in a final composite spectrum. A three-point running average of this final spectrum was made to reduce the effects of point scatter in the data. The peaks of known energy from the ThC'' spectrum were used to obtain an energy claibration curve containing both a linear term and a quadratic term which accounted for any non-linearity in the ADC. The center of the coincident γ-ray peaks was estimated and the energies of these peaks found from the calibration curve.

Chapter III

DATA ANALYSIS AND EXPERIMENTAL RESULTS

A. Method of Analysis

1. Gamma-Ray Angular Distribution Equations

The experimental method used for the α-γ correlation measurements and the method of theoretical analysis were primarily developed by Litherland and Ferguson. (15) The basis of their procedure is to exploit the simplifications brought about by making the reacting system in a nuclear reaction axially symmetric. A γ-ray emitting state formed in this way is aligned and can usually be described by a small number of population parameters for the magnetic substates of the residual nucleus. This type of alignment can be achieved in a nuclear reaction of the type $X(h_1, h_2)Y^*$, $Y^* \rightarrow Y + \gamma$ if h_2 is detected in a counter axially symmetric about the beam axis. This reaction is illustrated in Figure 7 where it is schematically presented in the form

$$a\ \ell_1\ s_1 \rightarrow b \rightarrow J_1\ \ell_2\ s_2 \quad .$$

Here a and b symbolize, respectively, the spin of the target nucleus X

Figure 7. Schematic Reaction-Angular Momenta Diagram.

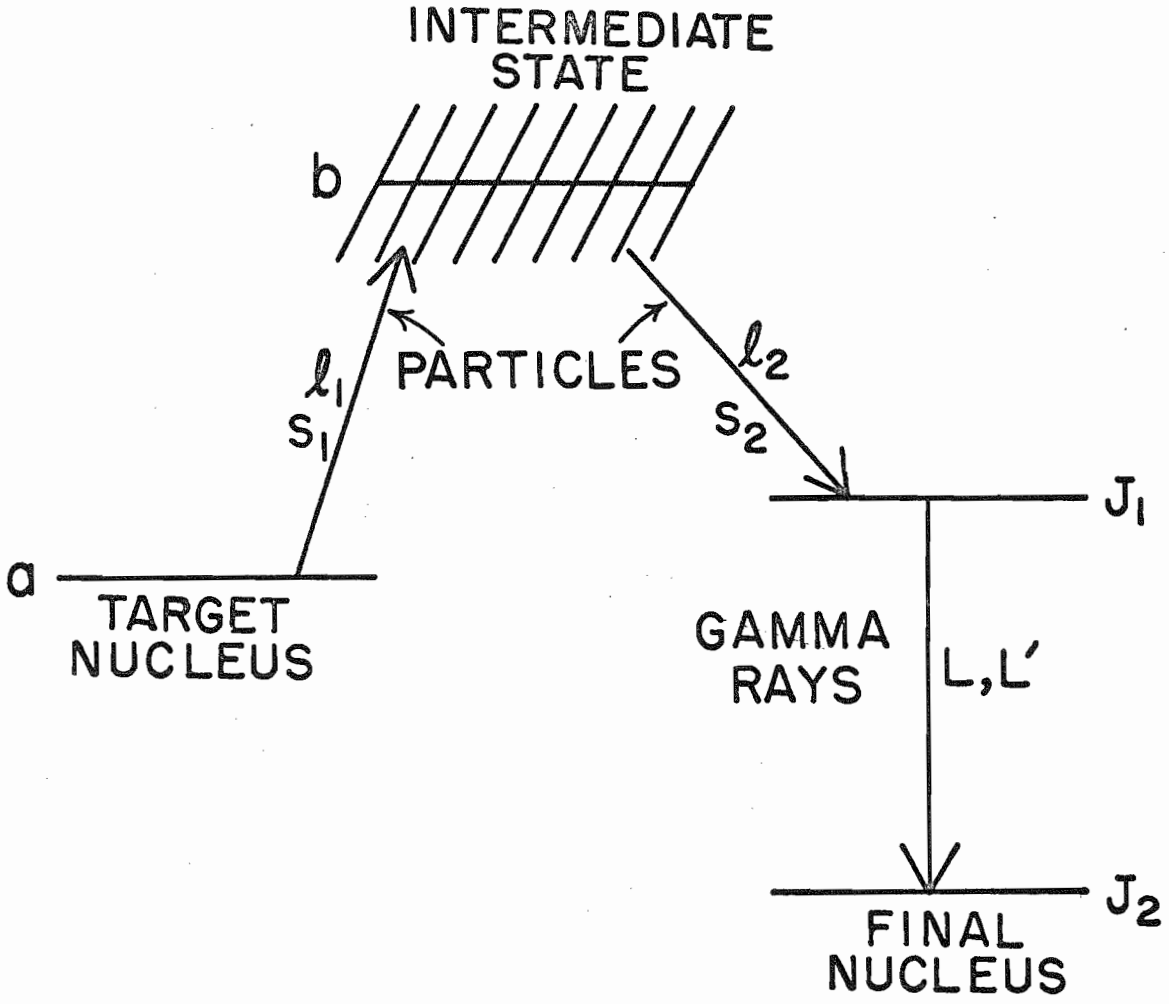
INTERMEDIATE
STATE
b
ℓ_1
S_1
PARTICLES
ℓ_2
S_2
J_1
a
TARGET
NUCLEUS
GAMMA
RAYS
L,L'
J_2
FINAL
NUCLEUS

and the spin of some intermediate state assumed to be formed in the reaction. The state b is usually not a level of sharp spin and parity but is normally several overlapping levels. The spin of the γ-ray emitting state Y* is symbolized by J_1 and that of the final state by J_2. The orbital angular momentum and intrinsic spin of the incident and emergent particles, h_1 and h_2, respectively, are represented by the symbols ℓ_1, s_1, ℓ_2, and s_2. The interfering multipolarities of the de-excitation γ rays are denoted by L and L'. The incident particle is assumed to be unpolarized. The axis of quantization is taken to be the beam axis. The appropriate angular momentum relations for this reaction are

$$\begin{aligned} \vec{R}_1 &= \vec{a} + \vec{s}_1 , \\ \vec{b} &= \vec{R}_1 + \vec{\ell}_1 = \vec{R}_2 + \vec{\ell}_2 , \\ \vec{R}_2 &= \vec{J}_1 + \vec{s}_2 \end{aligned} \qquad (1)$$

and

where $\vec{R}_1$ and $\vec{R}_2$ are the outgoing channel spins. From conservation of angular momentum the spin of the γ-ray emitting state, Y*, is

$$\vec{J}_1 = \vec{a} + \vec{s}_1 + \vec{\ell}_1 - \vec{s}_2 - \vec{\ell}_2 \quad . \qquad (2)$$

If the state Y* is formed by the absorption of an unpolarized particle in the direction of the quantization axis (the beam axis) and followed by the emission of a second particle which is detected along this same axis, then the magnetic substates of the final state which can be populated do not exceed the sum of the spins of X, h_1, and h_2. This theorem follows from the fact that the orbital angular momentum contained in plane waves in the direc-

tion of the beam axis has zero projection along this axis. This is clear since the orbital angular momentum of a particle, $\vec{\ell} = \vec{r} \times \vec{p}$, is always perpendicular to the linear momentum $\vec{p}$ and hence has zero projection on the $\vec{p}$ axis. This same point can be obtained if the incident and emergent beams are treated as plane waves and expanded in spherical harmonics $Y_m^{\ell}(\cos\theta)$. Then with $\theta = 0^{\circ}$ or 180° the only contributing terms to this expansion are those for which $m = 0$, i.e., zero projection. If the magnetic quantum numbers of the γ-ray emitting state of spin J_1 are denoted by a, then from Equation 2 with ℓ_1 and ℓ_2 equal to zero along the beam axis the maximum value of a is

$$a_{max} = a + s_1 + s_2 \ . \tag{3}$$

This equation is the basis for the previous comment that an aligned state may be described by a small number, depending on the reaction producing the alignment, of population parameters for the magnetic substates of the residual nucleus.

Litherland and Ferguson (15) give the expression for the angular distribution of a primary γ ray originating from a nucleus aligned in the manner described. Poletti and Warburton (43) have presented the identical relation in a form which is more amenable to analysis and it is this formulation which will be presented here.

The angular distribution of a γ ray which decays from a state of spin J_1 and magnetic quantum numbers a to a state of spin J_2 is given by

$$W(\theta) = \sum_k a_k \; P_k(\cos\theta) = \sum_k \rho_k(J_1) F_k(J_1 J_2) \, Q_k \, P_k(\cos\theta) \qquad (4)$$

where θ is the angle between the beam axis and the direction of emission of the γ rays. The $P_k(\cos\theta)$ is a Legendre polynominal and the summation index k assumes even values from 0 to $2J_1$. The $\rho_k(J_1)$ are statistical tensors which describe the alignment of the initial state and the $F_k(J_1 J_2)$ depend only upon the γ-ray cascade. The Q_k are attenuation coefficients for the γ-ray detector. The calculation of these quantities for the present study, outlined in Reference 32, yielded the values 1.0, 0.9315, 0.7858, 0.5929, and 0.3882 for k ranging from 0 to 8, respectively.

The $\rho_k(J_1)$ are given by a weighted sum over the population parameters, P(a), of the $2J_1 + 1$ magnetic substates associated with J_1:

$$\rho_k(J_1) = \sum_a \rho_k(J_1, a) \, P(a) \qquad (5)$$

where a extends from $-J_1$ to J_1. The P(a) specify the fraction of aligned nuclei in the magnetic substates of J_1 and have the important restriction that they must be positive. The normalization is such that $\sum_a P(a) = 1$ so that the P(a) lie in the range $0 \leq P(a) \leq 1/2$ if the a_{max} of Equation 3 are non-zero. The $\rho_k(J_1, a)$ in Equation 5 are given by the ratio $\langle J_1 a, \, J_1 - a \mid k 0 \rangle \; / \; \langle J_1 a, \, J_1 - a \mid 00 \rangle$. The state J_1 is assumed to be unpolarized so that P(a) = P(-a) and the γ-ray angular distributions from the $\pm$ a magnetic substates are identical.

The γ-ray angular distribution from the state J_1 is assumed

to contain multipolarities L and L' where L and L' take on integer values from $|J_1 - J_2|$ to $J_1 + J_2$. If only the two lowest allowed multipole admixtures are assumed to be present in the γ-ray transition, as is assumed in this study, then the $F_k(J_1J_2)$ of Equation 4 are given by

$$F_k(J_1J_2) = \frac{F_k(LL\,J_2J_1) + 2x\,F_k(LL'\,J_2J_1) + x^2\,F_k(L'L'\,J_2J_1)}{1 + x^2} \qquad (6)$$

where L is the lowest allowed value and L' = L + 1. The multipole mixing ratio, x, is given by the ratio of reduced matrix elements:

$$x = \langle J_2 \| L' \| J_1 \rangle \Big/ \langle J_2 \| L \| J_1 \rangle \,. \qquad (7)$$

The $F_k(LL'\,J_2J_1)$ of Equation 6 are tabulated functions given in Reference 43. These coefficients further limit k to $k \leq \min(2L, 2L', 2J_1)$.

The phase convention for x chosen here is Convention II of Poletti and Start (7) which results from choosing a positive sign for the term linear in x in Equation 6. This convention, opposite to that of Reference 15 and 43, was chosen as a result of the careful study of phases of mixing ratios carried out by Poletti and Start concerning γ-ray transitions from the first two excited states of ^{21}Ne, ^{21}Na, and ^{23}Na. The phases obtained for ^{23}Mg should then be more readily compared with the phases found for the other N or Z = 11 nuclei. Rose and Brink (44) have recently treated the whole problem of the phases of mixing ratios by making a phase consistent derivation of angular distributions for γ rays emitted in the decay of an aligned

nuclear state.

Using Convention II the phases of the mixing ratios reported in this work are given assuming that the multipole mixture is a "natural one", i.e., a mixed E(L + 1) + ML transition, regardless of the known or suspected nature of the radiation. The phases of M 2 + E 1 mixtures presented here therefore are of the wrong sign and account must be taken of this when comparing these phases with theoretical predictions.

The angular distribution of the second γ ray in a cascade of the type $J_1 \rightarrow J_2 \rightarrow J_3$ with the first γ ray unobserved is given as

$$W(\theta) = \sum_k \rho_k(J_1)\, U_k(J_1 J_2)\, F_k(J_2 J_3)\, Q_k\, P_k(\cos\theta) \qquad (8)$$

where for the two lowest allowed multipolarities

$$U_k(J_1 J_2) = \frac{U_k(L J_1 J_2) + x^2\, U_k(L' J_1 J_2)}{1 + x^2} \quad . \qquad (9)$$

The $U_k(L J_1 J_2)$ are tabulated functions (43) and the other quantities have been previously defined.

2. Data Fitting Procedure

In the $^{24}Mg(^3He, \alpha)\,^{23}Mg$ reaction with the α particles detected at 180° with respect to the beam direction it is clear from Equation 3 that only the $\alpha = \pm 1/2$ magnetic substates of ^{23}Mg can be populated and each component is assumed to be equally populated. The angular correlations of the de-excitation γ rays are, for this situation, independent of the details of the formation of the excited states of ^{23}Mg. Consequently, the

angular distribution coefficients, i.e., the a_k coefficients of Equation 4, depend, essentially, only upon the spins of the levels of ^{23}Mg and the γ-ray mixing ratios.

The measured γ-ray angular distribution for a transition of the type $J_1 \rightarrow J_2$ was fitted with the theoretical distribution given in Equation 4 using a linear least-squares fitting code run on the DDP-224 computer. In this procedure the spins J_1 and J_2 take on all allowed values and for a given set of spins the fit is made for discrete values of x. The best fit corresponds to that value (or values) of x which minimizes χ^2 where

$$\chi^2 = \frac{1}{n}\sum_i \left[\frac{Y(\theta_i) - W(\theta_i)}{\Delta Y(\theta_i)}\right]^2 . \qquad (10)$$

In this equation $\Delta Y(\theta_i)$ is the statistical uncertainty assigned to the γ-ray yield $Y(\theta_i)$ at angle θ_i and n is the number of degrees of freedom. This latter quantity is given by the number of data points less the number of variable parameters which for the present case is the normalization between $Y(\theta)$ and $W(\theta)$. The mixing ratio is not considered to be a variable parameter in the fit since x is fixed for each calculation of χ^2. A plot of χ^2 versus x will then show dips corresponding to possible solutions for the assumed spins J_1 and J_2. The relative probability that a particular set of J_1, J_2, and x is the correct solution can be found by referring to χ^2-probability tables. (45) In this study for a fit to be regarded as an acceptable one, a value of χ^2 corresponding to a confidence level of

0.1% or greater had to be achieved. For five angles, n = 4 and $\chi^2(0.1\%) = 4.6$.

Since the limits on x are $\pm \infty$ the variable used in the fitting procedure was arctan x which was varied in 5° steps from -85° to 85°. Each minimum in the χ^2 curves was then studied by varying arctan x in 1° steps. The computer program could only accept one set of data at a time but could treat transitions of the type $J_1 \rightarrow J_2 \rightarrow J_3$. In this case the correlation of one of the γ rays of the cascade is fitted using Equation 8 with the mixing ratio of the unobserved γ ray fixed. In order to present the experimental data in a compact form the program initially fitted each angular correlation with a Legendre polynominal expansion of the form

$$W(\theta) = a_0 + a_2 P_2(\cos\theta) + a_4 P_4(\cos\theta) \quad . \tag{11}$$

The a_0 coefficients generated by this least-squares fit were used in conjunction with tables of efficiences and photopeak fractions for γ rays detected in Na(Tl) crystals (46) to obtain branching ratios for the decay modes of ^{23}Mg.

The statement that only the $a = \pm 1/2$ substates of ^{23}Mg are populated using the ^{24}Mg(^{3}He, α)^{23}Mg with collinear geometry is not quite true. The ^{3}He beam from the accelerator has a finite emittance which implies that not all of the ^{3}He ions impinging upon the target will be going in exactly the same direction, i.e., some of the particles will have a projection of orbital angular momentum along the beam axis. In addition, the

annular counter is not an ideal counter located at 180° with respect to the beam direction but is an annulus whose inner and outer edges subtend angles of 177° and 173°, respectively, at the target center. Litherland and Ferguson (15) have considered these effects which, for the present case, allow magnetic substates with $\alpha > 1/2$ to be populated. Their results indicate that the population of the $\alpha = \pm 3/2$ substates should be proportional to $l^2\epsilon^2$ where l is the orbital angular momentum of the ^{3}He beam and ϵ is the half angle in radians subtended by the annular counter at the target center. This result reflects the fact that the response of the system is proportional to the approximate area of the counter, i.e., $\pi\epsilon^2$. With $\epsilon = 0.015$ radians and $l = 2$ there should be approximately a 5% population of the $\alpha = \pm 3/2$ substates. To investigate this effect the χ^2 test was performed first with $P(3/2) = 0$. The minima in the resulting χ^2 curves were then studied by fitting the data with $P(3/2) = 0.05\ P(1/2)$. This procedure was followed in fitting each of the angular correlations and the so called Finite Size Effect (FSE) was found to be negligible.

B. Experimental Results

1. General

For convenience in discussing the experimental results the levels of ^{23}Mg will be labeled by numbers beginning with 0 for the ground state. The mention of the parameter x_{10}, for example, will then refer to the mixing ratio of the γ ray for the transition from the first-excited state (1) to

the ground state (0). The symbol J will refer to the total angular momentum (spin) of the initial nuclear state in a transition. For cases where more than one transition is involved the symbol J will be labeled with the number of the particular level being discussed. The phases of mixing ratios presented here will be strictly experimental phases and will conform to Convention II. (7) The ^{23}Mg level scheme was taken from the work of Hinds and Middleton (8) who studied the ^{24}Mg(^{3}He, α)^{23}Mg reaction using a broad-range magnetic spectrometer to detect the α particles. Spins of 11/2 or greater were not considered in the following analysis as they are not expected on the basis of the systematics of neighboring nuclei and because they would lead to level lifetimes incompatible with the effective resolving time of the coincidence circuit. This last remark will be discussed in Section 3.

2. The ^{23}Mg Ground State

Most of the published information concerning the ^{23}Mg ground state has been summarized by Endt and Van der Leun. (47) The ^{23}Mg nucleus is radioactive with a half-life of 12 s. The β^{+}-decay proceeds mainly to the ^{23}Na ground state with approximately 91% intensity. This decay is super-allowed (log ft = 3.7) which determines the ground-state spin and parity of ^{23}Mg as $J^{\pi} = 3/2^{+}$. Gamma-annihilation coincidence measurements indicate a 9% branch to the ^{23}Na 0.44-MeV first-excited state with log ft = 4.5. The a_0 angular distribution from the ^{24}Mg(^{3}He, α)^{23}Mg reaction has been measured at ^{3}He energies of 5.5 MeV (10), 10 and

12 MeV (24), and at 15 MeV. (16) The analysis of these angular distributions leads to an $\ell_n = 2$ assignment for the picked-up neutron and a $J^\pi = (3/2, 5/2)^+$ assignment to the ground state. The d_o angular distribution from the ^{24}Mg(p, d) ^{23}Mg reaction has been measured at $E_p = 33.6$ MeV and is also characterized by $\ell_n = 2$ in agreement with the (^{3}He, α) results. (18) In the following analysis the ground state spin of ^{23}Mg will be assigned $J^\pi = 3/2^+$. The mirror nucleus ^{23}Na also has $J^\pi = 3/2^+$ for the ground state as does ^{21}Ne and ^{21}Na. (6)

3. The 0.451-MeV Level

The decay of the 0.451-MeV first-excited state was studied at ^{3}He bombarding energies of 6.37 and 8.05 MeV. A typical coincidence decay spectrum recorded in the NaI crystal is shown in Figure 8. From the spectrum recorded with the Ge(Li) detector, the energy of this transition was found to be 0.451 ± 0.004 MeV in agreement with the value 0.451 ± 0.010 MeV given in Ref. 8. Two separate angular correlations taken at a ^{3}He energy of 6.37 MeV and one taken at 8.05 MeV were each fitted by the method of least squares with a Legendre polynominal expansion including even terms up to $P_4(\cos\theta)$. The average value of the coefficients of $P_2(\cos\theta)$ and $P_4(\cos\theta)$ from the three measurements was $a_2/a_o = -0.46 \pm 0.02$ and $a_4/a_o = -0.02 \pm 0.02$. The errors given here are statistical. No finite geometry corrections were made in obtaining these coefficients.

Figure 8. The 0.451-MeV Level Gamma-Ray Decay Spectrum. This figure illustrates the spectrum of γ rays observed at 26° to the beam in coincidence with α particles leading to the ^{23}Mg 0.451-MeV level in the ^{24}Mg(^{3}He, $\alpha\gamma$)^{23}Mg reaction at a ^{3}He energy of 6.37 MeV. The solid circles represent true coincidences and the open circles represent accidental coincidences. A true-to-accidental ratio of approximately four was obtained for this transition.

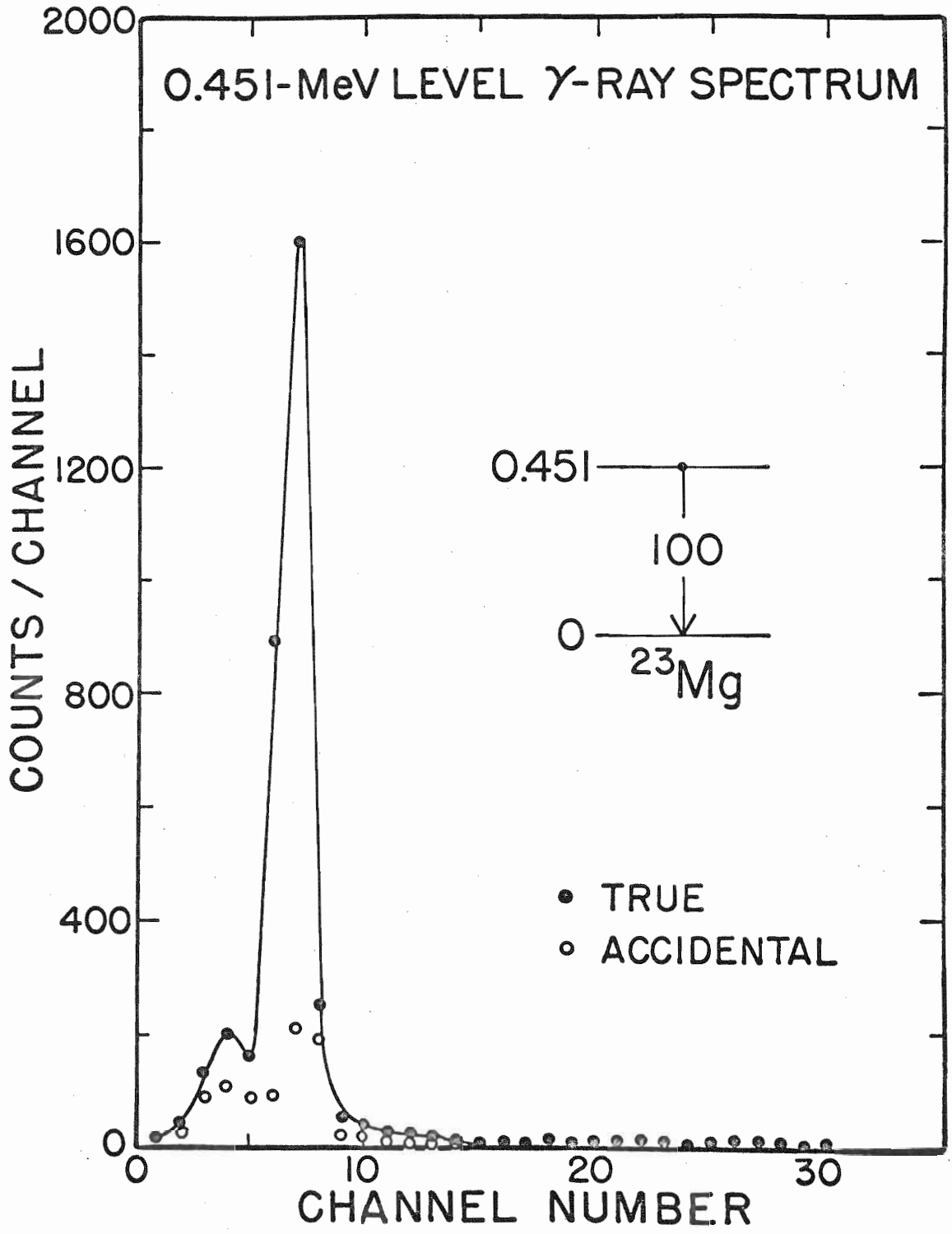
0.451-MeV LEVEL γ-RAY SPECTRUM
COUNTS / CHANNEL
CHANNEL NUMBER
2000
1600
1200
800
400
0
0
10
20
30
0.451
100
0
23Mg
TRUE
ACCIDENTAL

The large anisotropy observed eliminates J = 1/2 for this level and the absence of a marked $P_4(\cos\theta)$ term is incompatible with J = 7/2. Spin assignments of 9/2 or greater were not considered as probable for this level since the lifetime of the level would then be long compared with the resolving time of the coincidence circuit. Assuming for the moment that the 0.451-MeV level has J = 9/2, then the fastest possible transition would have E3 multipolarity. The Weisskopf estimate for such a transition, (48) using a radius of 1.2 f, leads to a mean lifetime of $\tau_m \approx 10^{-2}$ s. Including a factor of 100 for possible enhancement leads to an upper bound of $\tau_m \approx 10^{-4}$ s for the transition speed. The relative number of decaying nuclei remaining after a time t is e^{-t/τ_m}. With t equal to the effective resolving time of 10^{-8} s, the relative number of nuclei decaying during this time is quite small. In addition, the nuclear orientation of a level with $\tau_m \approx 10^{-4}$ s would not be expected to be preserved. Spins of 9/2 or greater are also excluded by an $\ell_n = 2$ assignment to this level, to be discussed later, and also on the basis of the systematics of neighboring nuclei. From these arguments the experimental data can only be satisfied by J = 3/2 or 5/2.

The χ^2 test was applied to each of the three correlations assuming J to be 1/2, 3/2, 5/2, and 7/2. Minima were found in each of the resulting curves although these solutions did not dip below the 0.1% confidence level. The fact that better fits were not achieved was believed to be due to instrumental difficulties associated with detecting this low-energy

γ ray. The χ^2 test only allows for statistical error whereas the statistics obtained for each of the correlations was quite good. Rather than average the mixing ratios obtained from the three separate fits, the three χ^2 curves were added together after weighing each with the appropriate number of degrees of freedom. Two of the angular correlations were taken at five angles to the beam (n = 4) and the third one at four angles (n = 3). The combined χ^2 was then taken to be

$$\chi^2 = (4/11)\chi_1^2 + (4/11)\chi_2^2 + (3/11)\chi_3^2 \qquad (12)$$

where χ_1^2, χ_2^2, and χ_3^2 are the individual χ^2 fits from the three correlations.

From the combined fit, shown in Figure 9, the most probable solutions are J = 5/2 with x_{10} = tan $(-4 \pm 3)^\circ$ (= -0.070 ± 0.052) and J = 3/2 with x_{10} = tan $(-62 \pm 5)^\circ$ (= -1.88 ± 0.09) or tan $(-42 \pm 5)^\circ$ (= -0.90 ± 0.09). The solutions for J = 1/2 and 7/2 are seen in the figure to be excluded with a high probability. The errors on x_{10} were calculated from the difference between the value of x_{10} found from the combined fit and the x_{10} values found from the individual fits using the method of weighted averages as discussed in the propagation of errors. (49) Without additional information, e.g., lifetime measurements, it is not possible to discriminate between the two solutions J = 3/2 and 5/2 for the 0.451-MeV level.

The a_1 angular distribution from the ^{24}Mg(^{3}He, a)^{23}Mg reaction has been measured at ^{3}He energies of 5.5 MeV (10), 10 and 12 MeV (24),

Figure 9. E_γ = 0.45-MeV Angular Correlation and Combined χ^2 versus Arctan X_{10} for the 0.451-MeV Level. The combined χ^2 was formed by summing the χ^2 fits to each of the three angular correlations measured for the 0.451-MeV level. Each χ^2 was weighted with the appropriate number of degrees of freedom as described in the text. Spins of J = 1/2, 3/2, 5/2, and 7/2 were assumed for the 0.451-MeV level with J = 3/2 and 5/2 yielding the most probable solutions. At the top of the figure is shown the angular correlation measured at a ^{3}He energy of 6.37 MeV. The solid line through these data is the fit for J = 5/2 and arctan $x_{10} = -4^\circ$. For each of the three fits P(3/2) = 0 with the FSE being insignificant. Note that the data are plotted as a function of $\cos^2\theta$.

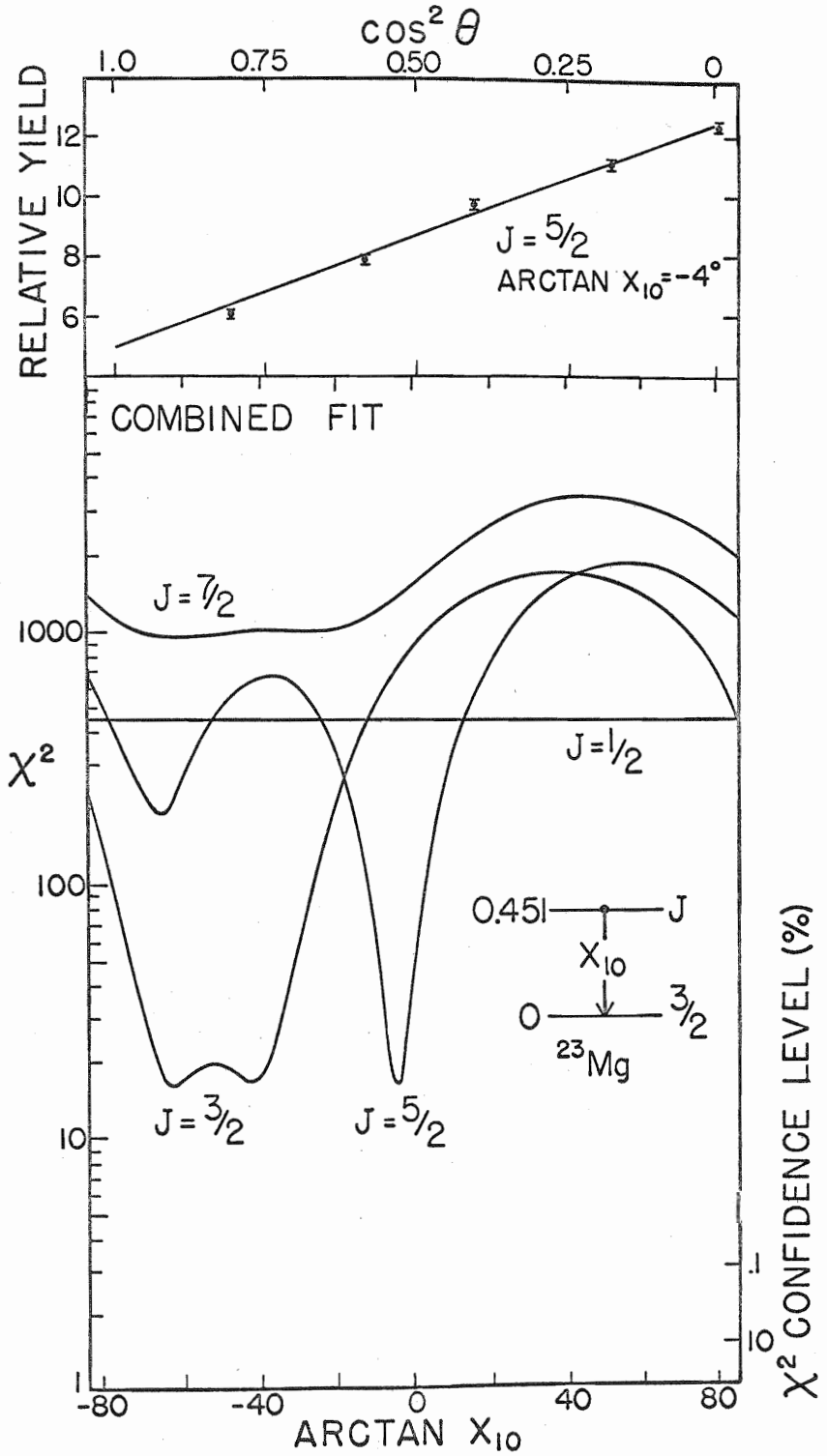
cos² θ
1.0
0.75
0.50
0.25
0
RELATIVE YIELD
12
10
8
6
J = 5/2
ARCTAN X10=-4°
COMBINED FIT
J = 7/2
1000
χ²
J = 1/2
100
0.451
J
X10
0
3/2
23Mg
J = 3/2
J = 5/2
10
1
-80
-40
0
40
80
ARCTAN X10
χ² CONFIDENCE LEVEL (%)
.1
.01

and at 15 MeV. (16) In each case the distribution was characterized by $\ell_n = 2$ which leads to a $J^\pi = (3/2, 5/2)^+$ assignment to the 0.451-MeV level. Dubois and Earwaker (24) report a noticeable difference in the shape of the a_o and a_1 angular distributions and remark that the effect may be due to a J-dependence of the pickup reaction. (50) Kozub (51) has measured the d_o and d_1 angular distributions from the $^{24}Mg(p, d)^{23}Mg$ reaction at $E_p = 33.6$ MeV and found that both distributions were characterized by $\ell_n = 2$. A J-dependence effect was observed which appeared as a difference in the overall slope of the differential cross-section versus angle curves for the two distributions. In contrast to ($^3He, a$) reactions, J-dependence effects in (p, d) reactions have been shown to be quite distinct and pronounced as demonstrated by the work of Glashausser (52) and Legg and Rost. (53) The work of Kozub thus lends strong support to a $J^\pi = 5/2^+$ assignment to the ^{23}Mg 0.451-MeV level.

Further support for this assignment comes from experiments on the analogous state in the mirror nucleus ^{23}Na. Poletti and Start (7) have made a rigorous $5/2^+$ assignment to the first excited state in ^{23}Na which differs by less than 50 keV from the energy of the ^{23}Mg 0.451-MeV level. They found that $x_{10} = 0.08 \pm -0.02$. It is interesting to note that the ^{21}Ne first excited state at 0.35 MeV has $J^\pi = 5/2^+$ with $x_{10} = -0.08$ $\pm$ 0.03 (54) and the analogous level in ^{21}Na at 0.34 MeV has $J^\pi = 5/2^+$ with $x_{10} = 0.05 \pm 0.05$. (7) Additional support for the $5/2^+$ assignment comes from the theoretical prediction (55) that when collective effects

enhance the transition strengths for E2 radiations it is expected that E2/M1 mixing ratios for corresponding mirror transitions will most probably differ in sign. For a $5/2^+$ assignment the E2/M1 mixing ratio x_{10} in ^{23}Na and ^{23}Mg do indeed differ in sign whereas for a $3/2^+$ assignment the phase of x_{10} is negative for both nuclei.

4. The 2.904-MeV Level

The analysis of the angular correlations from the 2.904-MeV level will be presented at this time as it will permit a unique spin assignment of J = 5/2 for the 0.451-MeV level.

This level was studied at a ^{3}He energy of 6.37 MeV as the yield for this state, as shown in Figure 3, was greater than that for the nearby fourth and fifth excited states at 2.712 and 2.768 MeV, respectively. The contribution to the 2.904-MeV level γ-ray spectra from the low-energy portion of these two states was considered to be negligible. The coincident γ-ray spectrum, composed of nine spectra summed over five different angles to the beam, is shown in Figure 10. The 2.904-MeV level was found to decay (60 ± 4)% to the ground state and (40 ± 4)% to the first excited state. No γ rays resulting from the decay of the 2.712- and 2.768-MeV levels can be identified in this spectrum. A 2.75-MeV γ-ray spectral shape from a ^{24}Na source was used as a spectral shape for the 2.90-MeV γ ray in order to extract the 2.45-MeV γ ray. These branching ratios were obtained from the a_o coefficients of the Legendre polynominal fit to the 2.90- and 2.45-MeV angular correlations. The errors reflect

Figure 10. The 2.904-MeV Level Gamma-Ray Decay Spectrum. This figure illustrates the spectrum of γ rays in coincidence with the α group populating the ^{23}Mg 2.904-MeV level in the ^{24}Mg(^{3}He, $\alpha\gamma$)^{23}Mg reaction at a ^{3}He energy of 6.37 MeV. This spectrum is the sum of nine spectra taken at five different angles to the beam. The γ-ray peaks correspond to the transitions indicated in the decay scheme. A 2.90-MeV spectral shape, shown sketched in, was used to extract the 2.45-MeV γ ray. Accidental coincidences have been subtracted.

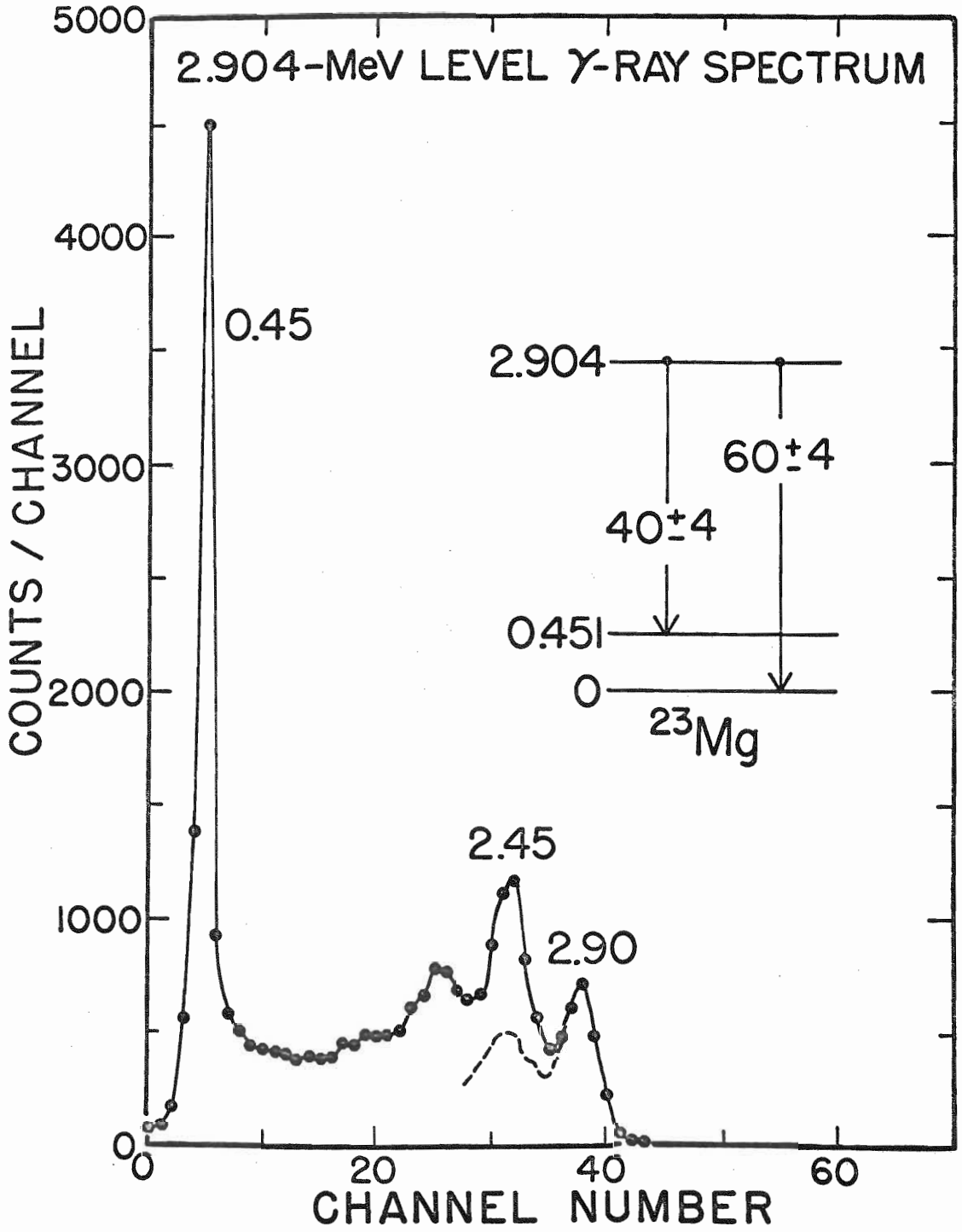
2.904-MeV LEVEL γ-RAY SPECTRUM
COUNTS / CHANNEL
CHANNEL NUMBER
5000
4000
3000
2000
1000
0
0
20
40
60
0.45
2.45
2.90
2.904
60±4
40±4
0.451
0
23Mg

both statistical uncertainty and the uncertainty in extracting the 2.45-MeV γ ray.

From the spectrum of γ rays detected at a ^{3}He energy of 8 MeV in the Ge(Li) detector, and in coincidence with α particles leading to the 2.712-, 2.768-, and 2.904-MeV levels, γ rays with energies of 2.902 ± 0.008 MeV and 2.454 ± 0.008 MeV could be identified as the primary transitions from the decay of the 2.904-MeV level. The 2.904-MeV value is in agreement with the value 2.904 ± 0.010 MeV given in Ref. 8 for the energy of the sixth excited state. This level was weakly populated at the ^{3}He energy of 8 MeV as shown in the Ge(Li) detector spectrum of Figure 20.

The 2.90-MeV angular correlation was anisotropic and was characterized by $a_2/a_0 = 0.11 \pm 0.03$ and $a_4/a_0 = 0.15 \pm 0.04$. When the χ^2 test was applied to this correlation, with assumed spins of J = 1/2, 3/2, 5/2, 7/2, and 9/2 for the 2.904-MeV level, only the solutions J = 3/2 with $x_{60} = \tan(-12 \pm 2)^\circ (= -0.213 \pm 0.035)$ and J = 5/2 with $x_{60} = \tan(14 \pm 2)^\circ (= 0.249 \pm 0.035)$ had a confidence level of 0.1% or less. The errors were taken to be the width of the χ^2 curve for a given J between the minimum and the 0.1% confidence level. This criterion was used to assign an error to x in all cases where a solution had a confidence level of less than 0.1%. The results of the χ^2 analysis and the experimental correlation are shown in Figure 11.

The 2.45-MeV correlation was anisotropic and was characterized by $a_2/a_0 = -0.05 \pm 0.05$ and $a_4/a_0 = -0.24 \pm 0.07$. When the χ^2

Figure 11. E_γ = 2.90-MeV Angular Correlation and χ^2 versus Arctan X_{60} for the 2.904-MeV Level. The data were fitted assuming J, the spin of the 2.904-MeV level, to be 1/2, 3/2, 5/2, 7/2, and 9/2, resulting in the five curves illustrated in the figure. Only the solutions for J = 3/2 and 5/2 are seen to have a confidence level of 0.1% or less. In the top portion of the figure is shown the 2.90-MeV correlation taken at a ^{3}He energy of 6.37 MeV. The solid lines through the data are the fits for J = 3/2 and 5/2 with specific multipole mixtures. The probabilities of χ^2 exceeding the 0.1%, 1%, and 10% confidence levels are 0.1%, 1%, and 10%, respectively, for a correct solution.

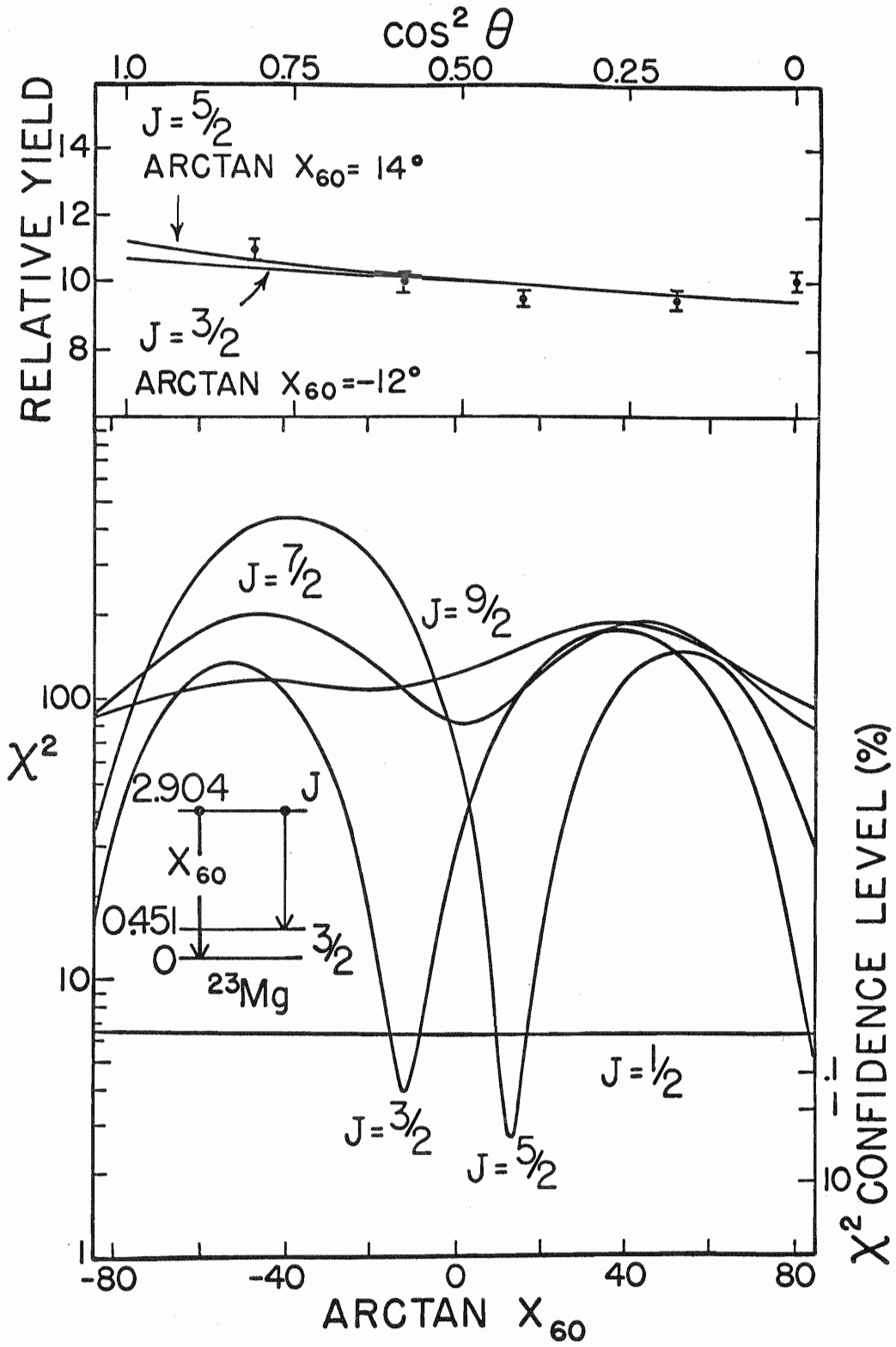
cos² θ
1.0
0.75
0.50
0.25
0
RELATIVE YIELD
14
12
10
8
J = 5/2
ARCTAN X60 = 14°
J = 3/2
ARCTAN X60 = -12°
J = 7/2
J = 9/2
100
χ²
2.904
J
X60
0.451
0
3/2
23Mg
10
J = 1/2
J = 3/2
J = 5/2
1
-80
-40
0
40
80
ARCTAN X60
χ² CONFIDENCE LEVEL (%)
10

test was applied to this angular distribution, the spin of the 0.451-MeV level was assumed to be $J_1 = 3/2$ or $5/2$ as determined from fitting the α_1-γ angular correlation discussed earlier. The spin of the 2.904-MeV level was then assumed to be $J = 3/2$ or $5/2$ as was just shown. The results of this analysis along with the experimental data are shown in Figure 12. For the spin sequence $J \rightarrow J_1 = 5/2 \rightarrow 3/2$, $x_{61} = \tan (10 \pm 3)^\circ (= 0.176 \pm 0.052)$ and for $3/2 \rightarrow 3/2$, $x_{61} = \tan (-15 \pm 5)^\circ (= -0.268 \pm 0.087)$ or $\leq \tan (-85)^\circ (\leq -11.43)$. For the sequence $J \rightarrow J_1 = 3/2 \rightarrow 5/2$, $x_{61} = \tan (-74 \pm 8)^\circ (= -3.49 \pm 0.14)$ or $\tan (-4 \pm 7)^\circ (= -0.070 \pm 0.123)$, and for $5/2 \rightarrow 5/2$, $x_{61} = \tan (-24 \pm 9)^\circ$ $(= -0.445 \pm 0.158)$ or $\tan (82 \pm 10)^\circ$ $(= 7.12 \pm 0.18)$.

In order to discriminate between the solutions $J_1 = 3/2$ and $5/2$ for the 0.451-MeV level, the 0.45-MeV cascade transition was extracted and was found to be characterized by $a_2/a_o = -0.27 \pm 0.02$ and $a_4/a_o = -0.01 \pm 0.03$. The procedure followed in fitting this correlation was to fix x_{61} at one of the values which gave an acceptable solution for the 2.45-MeV correlation and allow $\arctan x_{10}$ to take on discrete values between -85° and 85°. For a transition of this type the data are fitted with the theoretical correlation given in Equation 8. For a consistent solution, the values of x_{10} so obtained must agree with the values of x_{10} found from analysing the α_1-γ angular correlation. The results of this analysis are shown in Figure 13. In the left hand portion of this figure the spin of the 0.451-MeV level has been assigned $J_1 = 3/2$ and the spin of the 2.904-MeV

Figure 12. E_γ = 2.45-MeV Angular Correlation and χ^2 versus Arctan X_{61} for the 2.904-MeV Level. In the left hand portion of the figure the spin of the 0.451-MeV level was assumed to be $J_1 = 3/2$ and J, the spin of the 2.904-MeV level, was assumed to be 3/2 or 5/2 resulting in the two curves illustrated in the figure. Directly above these curves are the experimental data taken at a ^{3}He energy of 6.37 MeV. The solid lines through these data are the theoretical fits for J = 3/2 and 5/2 with specific mixing ratios. In the right hand portion of the figure is shown the results of a similar analysis but with $J_1 = 5/2$. Directly above these results are shown the experimental data and the fits for J = 5/2 and 3/2 with specific mixing ratios given in the figure.

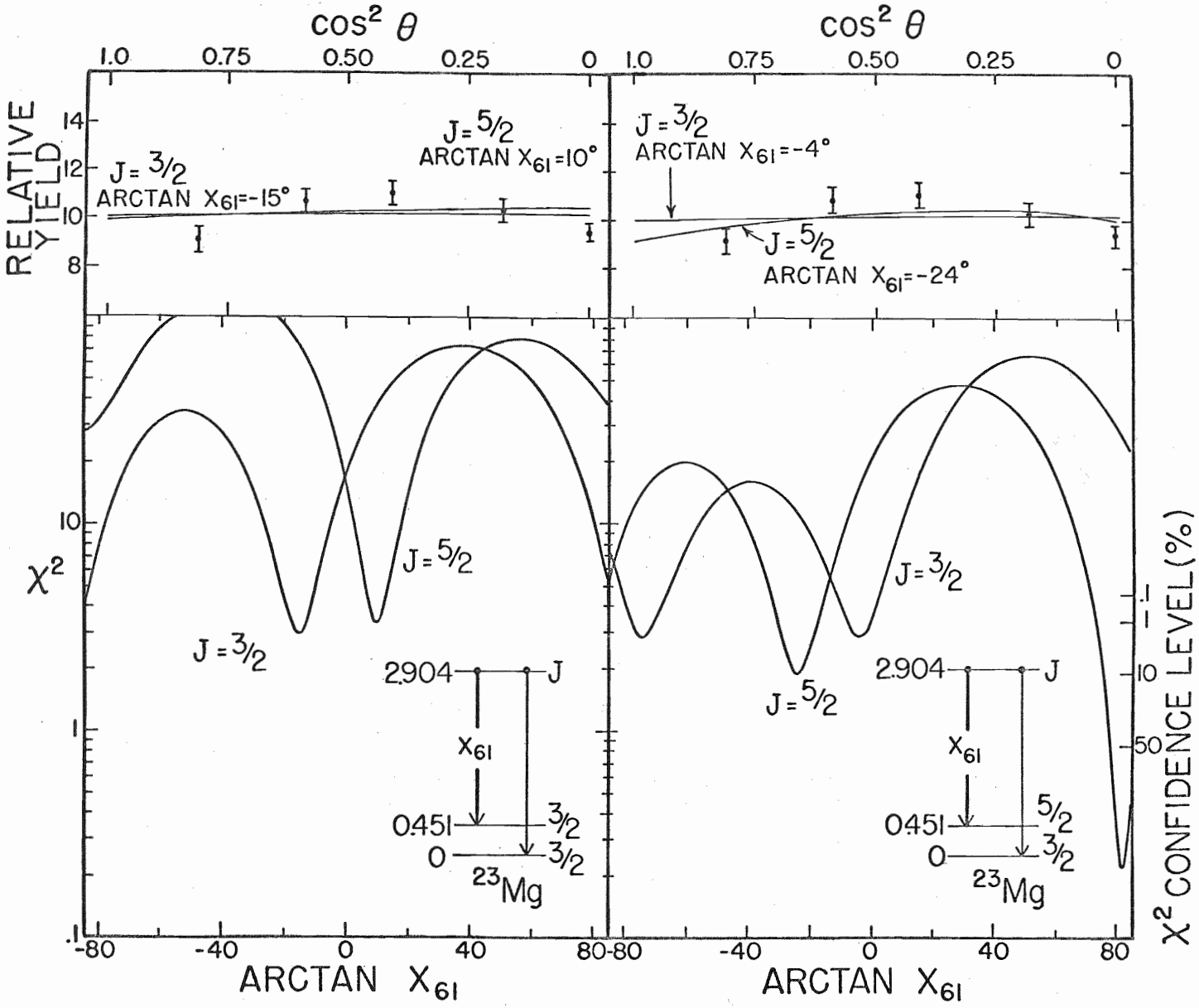
cos² θ
1.0
0.75
0.50
0.25
0
RELATIVE YIELD
J = 3/2
ARCTAN X61 = -15°
J = 5/2
ARCTAN X61 = 10°
J = 3/2
ARCTAN X61 = -4°
J = 5/2
ARCTAN X61 = -24°
χ²
J = 3/2
J = 5/2
2.904
J
X61
0.451
3/2
0
3/2
23Mg
J = 5/2
J = 3/2
2.904
J
X61
0.451
5/2
0
3/2
23Mg
χ² CONFIDENCE LEVEL (%)
ARCTAN X61
ARCTAN X61

Figure 13. E_γ = 0.45-MeV Angular Correlation and χ^2 versus Arctan X_{10} for the 2.904-MeV Level. In the left hand portion of the figure is shown the results of fitting the angular distribution of the 0.45-MeV cascade transition from the decay of the 2.904-MeV level with the spin of the 0.451-MeV level equal to 3/2. The mixing ratio x_{61} was fixed at a value found from fitting the 2.45-MeV correlation for J, the spin of the 2.904-MeV level, equal to 3/2 or 5/2. There is seen to be no value of x_{61} which yields a value of x_{10} consistent with that found from fitting the α_1-γ correlation (shown shaded). The solution for J = 5/2 and J_1 = 3/2 with x_{61} = tan $(10)^\circ$ yields a value of x_{10} with a confidence level of approximately 0.1% within the allowed range of x_{10}. In the right hand portion of the figure it is evident that a consistent solution is obtained if the spin of the 0.451-MeV level is 5/2, the confidence level being 50%.

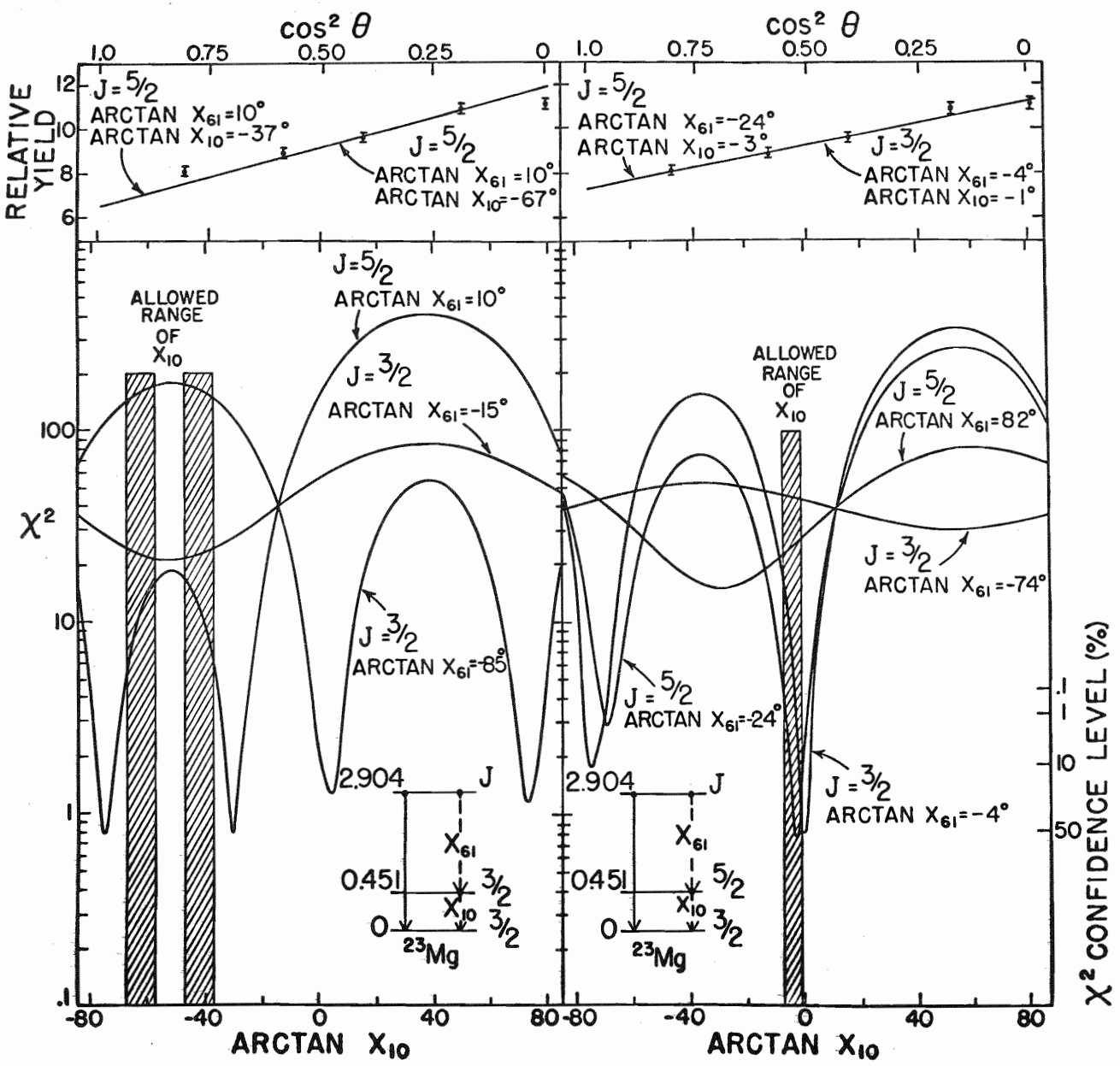
cos² θ
1.0
0.75
0.50
0.25
0
RELATIVE YIELD
J = 5/2
ARCTAN X61 = 10°
ARCTAN X10 = -37°
J = 5/2
ARCTAN X61 = 10°
ARCTAN X10 = -67°
J = 5/2
ARCTAN X61 = -24°
ARCTAN X10 = -3°
J = 3/2
ARCTAN X61 = -4°
ARCTAN X10 = -1°
ALLOWED RANGE OF X10
J = 5/2
ARCTAN X61 = 10°
J = 3/2
ARCTAN X61 = -15°
J = 3/2
ARCTAN X61 = -85°
J = 5/2
ARCTAN X61 = 82°
J = 3/2
ARCTAN X61 = -74°
J = 5/2
ARCTAN X61 = -24°
J = 3/2
ARCTAN X61 = -4°
χ²
2.904
J
X61
0.451
3/2
X10
0
3/2
23Mg
5/2
ARCTAN X10
χ² CONFIDENCE LEVEL (%)

level was assumed to be $J = 3/2$ and $5/2$. For these spin choices there is no value of x_{61} which yields a value of x_{10} for which the corresponding χ^2 has a confidence level of 0.1% or less within the range of x_{10} found from the α_1-γ angular correlation. Recall that for $J_1 = 3/2$ the α_1 - γ angular correlation, when fitted, yielded $x_{10} = \tan(-62 \pm 5)^\circ$ or $\tan(-42 \pm 5)^\circ$. It is the arctangent of these values which is the "allowed range of x_{10}" shown shaded in the left hand portion of Figure 13. In the top left hand portion of this figure is shown the 0.45-MeV angular distribution. The solid line through these data are the fits for $J = 5/2$, arctan $x_{61} = 10^\circ$ and arctan $x_{10} = -37^\circ$ and -67°, the two fits being superimposed. The two values of arctan x_{10} used in these fits correspond to the smallest value of χ^2 for these solutions within the allowed range of x_{10}. In the right hand portion of Figure 13 is shown the results of the χ^2 analysis assuming that $J_1 = 5/2$. With J, the spin of the 2.904-MeV level, equal to 3/2 or 5/2 and using the values of x_{61} found for these spin choices from the 2.45-MeV correlation, it is seen that there are two solutions which are consistent with the allowed range of x_{10}. Recall that from applying the χ^2 test to the α_1 - γ correlation a solution was found for $J_1 = 5/2$ with $x_{10} = \tan(-4 \pm 3)^\circ$. The arctangent of this value is shown shaded in the right hand portion of Figure 13. The two solutions consistent with this result are $J = 3/2$ with $x_{61} = \tan(-4 \pm 7)^\circ$ and $J = 5/2$ with $x_{61} = \tan(-24 \pm 9)^\circ$. In the top right hand portion of the figure is shown the experimental data. The solid lines through these data are the fits for $J \rightarrow J_1 =$

$5/2 \rightarrow 5/2$ with arctan $x_{61} = -24^{\circ}$ and arctan $x_{10} = -3^{\circ}$, and $J \rightarrow J_1 = 3/2 \rightarrow 5/2$ with arctan $x_{61} = -4^{\circ}$ and arctan $x_{10} = -1^{\circ}$, the two fits being superimposed. The values of arctan x_{10} used in these fits correspond to the smallest value of χ^2 for these solutions within the allowed range of x_{10}.

These results demonstrate that $J = 5/2$ is the most probable spin for the 0.451-MeV level. This spin assignment is further supported by the firm $5/2^+$ assignment for the corresponding level in the mirror nucleus ^{23}Na, the J-dependence effect observed by Kozub, and by the approximate rule for the sign of E2/M1 mixtures for corresponding mirror transitions.

It should be mentioned that the 0.45-MeV radiation resulting from the decay of the 2.904-MeV level contains an unknown component of 0.51-MeV annihilation radiation. This radiation results primarily from true coincidences following pair production in material in the vicinity of the NaI crystal. No account was taken of this component when extracting the 0.45-MeV angular correlation. However, since it was possible to obtain a fit to the $a_6 - \gamma_{0.45}$ correlation which was consistent with that found from fitting the $a_1 - \gamma_{0.45}$ correlation, which did not contain any appreciable annihilation radiation, it was believed that the $a_6 - \gamma_{0.45}$ correlation was not seriously distorted by this source of radiation.

Dubois and Earwaker (24) have measured the a_6 angular distribution from the ^{24}Mg(^{3}He, α)^{23}Mg reaction at a ^{3}He energy of 10 MeV and found it to be characterized by $\ell_n = 2$ which leads to a $J^{\pi} = (3/2, 5/2)^+$

assignment to the 2.904-MeV level. The mirror-pair analog of this level in ^{23}Na is assumed to be the 2.98-MeV level. Many attempts have been made to determine the spin of this level and the results favor 3/2 only slightly over a 5/2 assignment. (7) Dubois (56) has measured the d_6 angular distribution from the ^{22}Ne(^{3}He, d)^{23}Na at a ^{3}He energy of 10 MeV. The distribution was characterized by $\ell_p = 2$ which implies $J^\pi = (3/2, 5/2)^+$ for the ^{23}Na 2.98-MeV level. The $3/2^+$ assignment is favored as a result of the approximate rule for E2/M1 mixtures discussed previously. For a $3/2^+$ assignment to the ^{23}Na 2.98-MeV level and to the ^{23}Mg 2.904-MeV level, the mixing ratios x_{60} differ in sign (7) whereas for a $5/2^+$ assignment to both levels the signs are identical.

5. The 2.048-MeV Level

The 2.048-MeV level was studied at a ^{3}He energy of 8.05 MeV as this level was weakly populated at other energies between 6 and 8 MeV as shown in Figure 4. The summed γ-ray decay spectrum, composed of seven spectra taken at five different angles to the beam, is shown in Figure 14. The dominant mode of decay is through the first excited state, (85 ± 3)%, with a ground state decay of (15 ± 3)%. These branching ratios were determined from the summed γ-ray coincidence spectrum and from the a_o coefficients of the Legendre polynominal fit to the 2.05-MeV and 1.60-MeV angular correlations. In analysing the 2.05-MeV decay spectrum, the 2.03-MeV γ ray from the ^{28}Si(d, $p_2\gamma$)^{29}Si reaction was used as a spectral shape to extract the 1.60-MeV γ ray. The ^{29}Si 2.03-MeV

Figure 14. The 2.048-MeV Level Gamma-Ray Decay Spectrum. This figure illustrates the spectrum of γ rays in coincidence with the α group populating the ^{23}Mg 2.048-MeV level in the ^{24}Mg(^{3}He,$\alpha\gamma$)^{23}Mg reaction at a ^{3}He energy of 8.05 MeV. This spectrum is the sum of seven spectra taken at five different angles to the beam. The γ-ray peaks correspond to the transitions indicated in the decay scheme. A 2.05-MeV spectral shape, shown sketched in, was used to extract the 1.60-MeV γ ray. Accidental coincidences have been subtracted. Note that the scale used to depict the 0.45-MeV γ ray has been reduced by a factor of two.

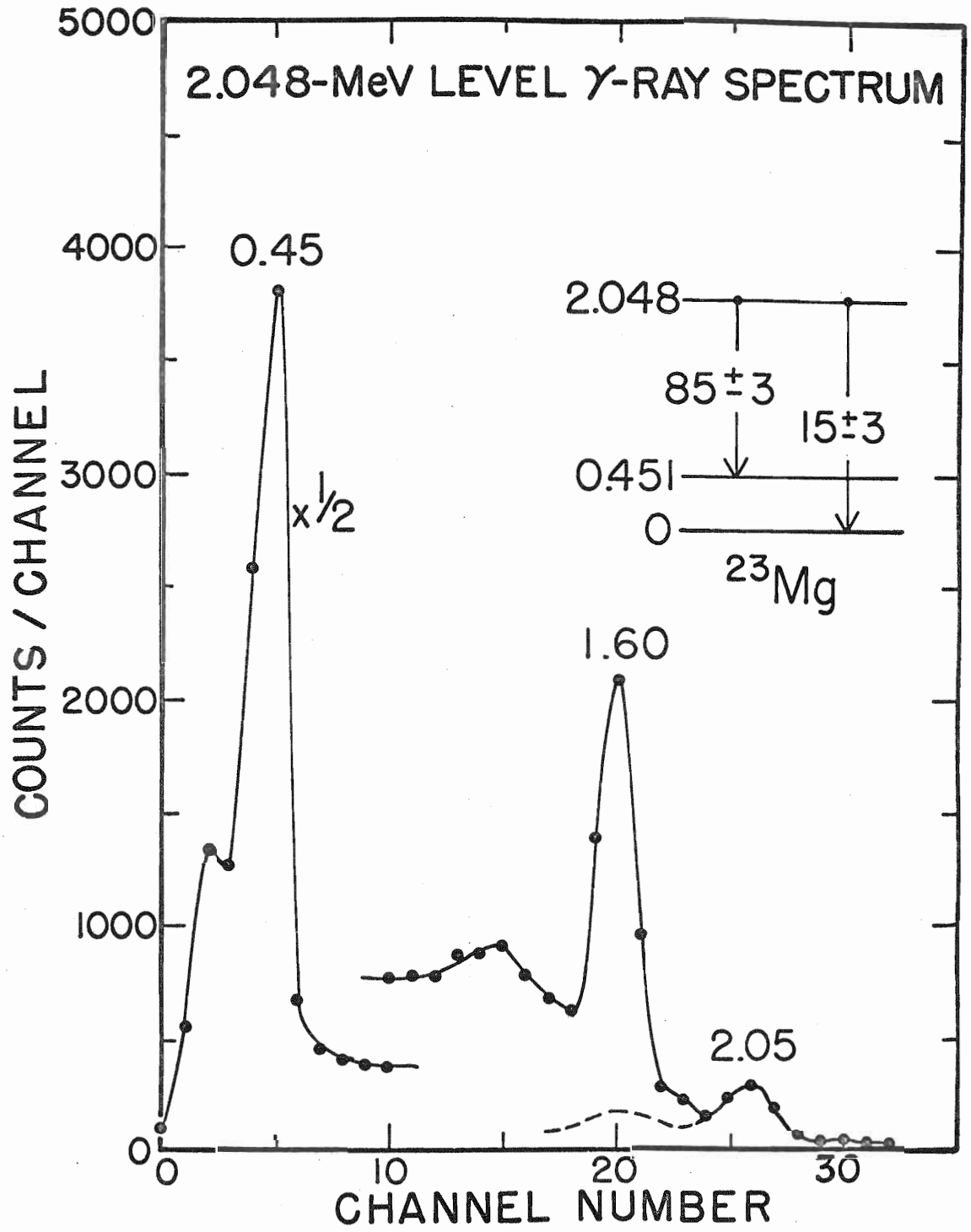
2.048-MeV LEVEL γ-RAY SPECTRUM
COUNTS / CHANNEL
CHANNEL NUMBER
0.45
x 1/2
1.60
2.05
2.048
85±3
15±3
0.451
0
23Mg
5000
4000
3000
2000
1000
0
0
10
20
30

level decays approximately 100% to the ground state. The error in the branching ratios reflects both statistical uncertainty and the uncertainty in extracting the 1.60-MeV γ ray.

From the spectrum of γ rays detected in the Ge(Li) detector at a ^{3}He energy of 8 MeV, and in coincidence with α particles populating the 2.048-MeV level, γ rays with energies of 0.451 ± 0.004 MeV and 1.599 ± 0.004 MeV were identified with transitions from the decay of the ^{23}Mg second-excited state. The ground state branch was too weak to be clearly discerned above the background. The two γ rays observed lead to an energy of 2.050 ± 0.006 MeV for the ^{23}Mg second-excited state in agreement with the result 2.048 ± 0.010 MeV given in Ref. 8.

The angular correlation of the 1.60-MeV γ ray was extracted using the 2.03-MeV spectral shape and was found to be characterized by $a_2/a_o = -0.66 \pm 0.03$ and $a_4/a_o = 0.01 \pm 0.04$ where these coefficients are the average values from three separate measurements. In the χ^2 analysis of this correlation the spin of the 0.451-MeV level was fixed at $J_1 = 5/2$ and the spin, J, of the 2.048-MeV level was allowed to assume values from 1/2 to 9/2. The resulting χ^2 curves from fitting one of the three angular correlations taken at a ^{3}He energy of 8.05 MeV are illustrated in the left hand portion of Figure 15. Solutions with confidence levels of 0.1% or less were found for $J = 7/2$ with $x_{21} = \tan(-10.3 \pm 2.2)^\circ$ $(= -0.182 \pm 0.038)$ or $J = 3/2$ with $x_{21} = \tan(33.3 \pm 3.0)^\circ (= 0.657 \pm 0.052)$ or $\tan(68.3 \pm 3.0)^\circ (= 2.51 \pm 0.05)$. These mixing ratios are the weighted

Figure 15. E_γ = 1.60-, 0.45-MeV Angular Correlations and χ^2 versus Arctan X_{21}, Arctan X_{10} for the 2.048-MeV Level. In the left hand portion of the figure is shown the results of fitting one of the three measured 1.60-MeV correlations with $J_1 = 5/2$ and $J = 1/2$ through 9/2. Spins of $J = 7/2$ and 3/2 are seen to yield acceptable solutions. One of the sets of data taken at a ^{3}He energy of 8.05 MeV is shown in the top portion of the figure. The solid line through these data is the theoretical fit for $J = 7/2$ and $x_{21} = \tan(-10)^\circ$. In the right hand portion of the figure is shown the results of fitting one of the 0.45-MeV cascade transitions with x_{21} fixed at the average values given in the text. The shaded region is the range of x_{10} determined from the analysis of the $\alpha_1 - \gamma_{0.45}$ correlation with $J_1 = 5/2$, i.e., $x_{10} = \tan(-4 \pm 3)^\circ$. It is estimated that the $J = 7/2$ solution is approximately 80 times more consistent with this result than is the solution for $J = 3/2$. One of the 0.45-MeV correlations is shown at the top of the figure with the fits for $J = 7/2$ (solid line) and 3/2 (dashed line) with specific multipole mixtures.

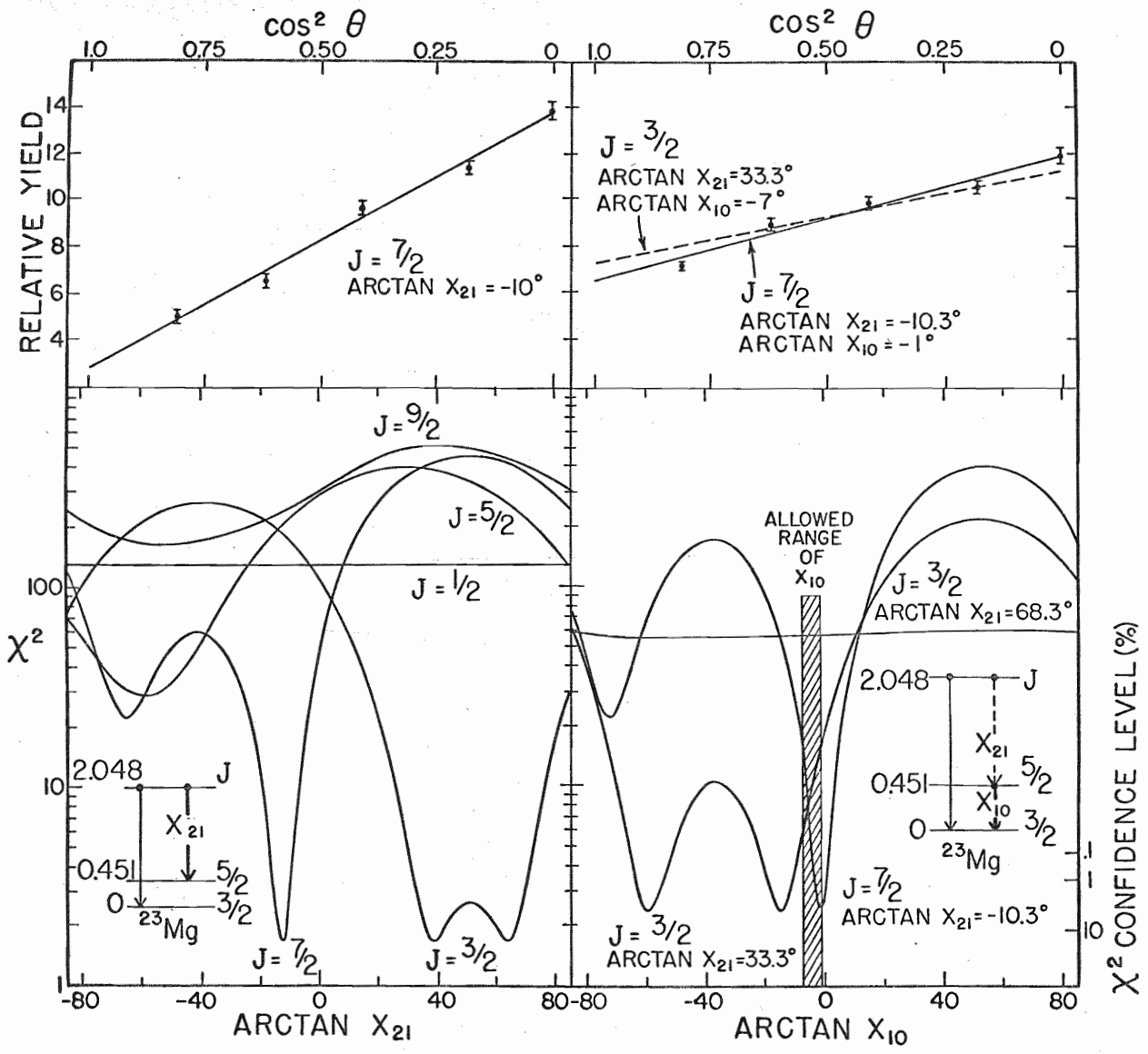
cos² θ
1.0
0.75
0.50
0.25
0
RELATIVE YIELD
J = 7/2
ARCTAN X21 = -10°
J = 3/2
ARCTAN X21=33.3°
ARCTAN X10=-7°
J = 7/2
ARCTAN X21 = -10.3°
ARCTAN X10 = -1°
J = 9/2
J = 5/2
J = 1/2
χ²
100
10
1
2.048
J
X21
0.451
5/2
0
3/2
23Mg
J = 7/2
J = 3/2
ALLOWED RANGE OF X10
J = 3/2
ARCTAN X21=68.3°
J = 3/2
ARCTAN X21=33.3°
J = 7/2
ARCTAN X21=-10.3°
X10
-80
-40
0
40
80
ARCTAN X21
ARCTAN X10
χ² CONFIDENCE LEVEL (%)
.1
10

averages of three measurements and were calculated using the procedure given in the discussion of the propagation of errors in Ref. 49.

In order to obtain discrimination against either the J = 7/2 or 3/2 solutions the 0.45-MeV cascade correlation was extracted and was characterized by $a_2/a_o = 0.35 \pm 0.02$ and $a_4/a_o = -0.04 \pm 0.03$. In analysing this angular distribution the mixing ratio x_{21} was fixed at the values which gave acceptable solutions for the 1.60-MeV correlation and the mixing ratio x_{10} was allowed to vary. For a consistent solution the values of x_{10} so obtained must again agree with the value of x_{10} found from fitting the $\alpha_1 - \gamma_{0.45}$ angular correlation. These results are shown in the right hand portion of Figure 15. Only the solution for J = 7/2 with $x_{21} = \tan(-10.3)^\circ$ yields a χ^2 with a confidence level of 0.1% or less within the allowed range of x_{10}, shown shaded. For J = 3/2 and $x_{21} = \tan(33.3)^\circ$ the minimum value of χ^2 within the allowed range of x_{10} is 6 which corresponds to a confidence level of approximately 0.05%. The minimum value of χ^2 for J = 7/2 within the allowed range of x_{10} has a confidence level of 4%. Therefore J = 7/2 is approximately 80 times more probable than is 3/2 for the spin of the 2.048-MeV level. The fits to one of the three measured 0.45-MeV correlations is shown in the top right hand protion of Figure 15. For these fits the values of x_{21} used are the weighted average of three measurements and the x_{10} values correspond to the smallest value of χ^2 for the solutions within the allowed range of x_{10}.

The 2.05-MeV transition, though weak, was extracted with con-

siderable difficulty. The angular distribution was found to be characterized by $a_2/a_o = 0.17 \pm 0.10$ and $a_4/a_o = -0.33 \pm 0.15$. These coefficients are only consistent for a spin of 5/2 or greater for the 2.048-MeV level and support the results above that J = 7/2 is more probable than J = 3/2. The χ^2 curves for J = 7/2 and 3/2 for one of the sets of experimental data taken at a ^{3}He energy of 8.05 MeV are shown in Figure 16. For J = 7/2, $x_{20} = \tan(-8 \pm 14)^\circ (= -0.141 \pm 0.249)$ and for J = 3/2, $x_{20} = \tan(-6 \pm 13)^\circ$ $(= -0.105 \pm 0.231)$. Unfortunately, both solutions have a confidence level of approximately 10% which negates the above argument concerning the a_2 and a_4 coefficients. The large statistical uncertainty in the data is seen to introduce a large error in x_{20}. The x_{20} value for J = 7/2 conflicts with an earlier measurement in this laboratory (21) which yielded an improbably large ($x_{20} = \tan(-25 \pm 3)^\circ$) mixing ratio for this transition, if the parity of the level is positive, although this fit led to an unambigious J = 7/2 assignment to the 2.048-MeV level. The present result, $x_{20} = \tan(-8 \pm 14)^\circ$, is favored. DaSilva et al. (23) have fitted this same correlation and report $x_{20} = 0.06 \pm 0.05$ for J = 7/2. The weighted average (49) of the two results is $x_{20} = 0.05 \pm 0.05$. This small value of x_{20} suggests that the multipolarity of the ground state decay is M3 + E2 which would lead to a $\pi = +$ assignment to the 2.048-MeV level. Dubois and Earwaker (24) obtained a good $\ell_n = 4$ fit to the a_2 angular distribution which leads to $J^\pi = (7/2, 9/2)^+$ for this level. However, they remark that the fit may be fortuitous since the level is not strongly populated in the (^{3}He, a) reaction.

Figure 16. E_γ = 2.05-MeV Angular Correlation and χ^2 versus Arctan X_{20} for the 2.048-MeV Level. This figure shows the χ^2 fits to the 2.05-MeV angular distribution with J = 7/2 and 3/2. In the top portion of the figure is shown the experimental correlation taken at a ^{3}He energy of 8.05 MeV. The solid line through these data is the fit for J = 7/2 with x_{20} = tan $(-8)^\circ$ and the dashed line is the fit for J = 3/2 with x_{20} = tan $(-6)^\circ$. The 7/2 fit appears to be slightly better than that for J = 3/2.

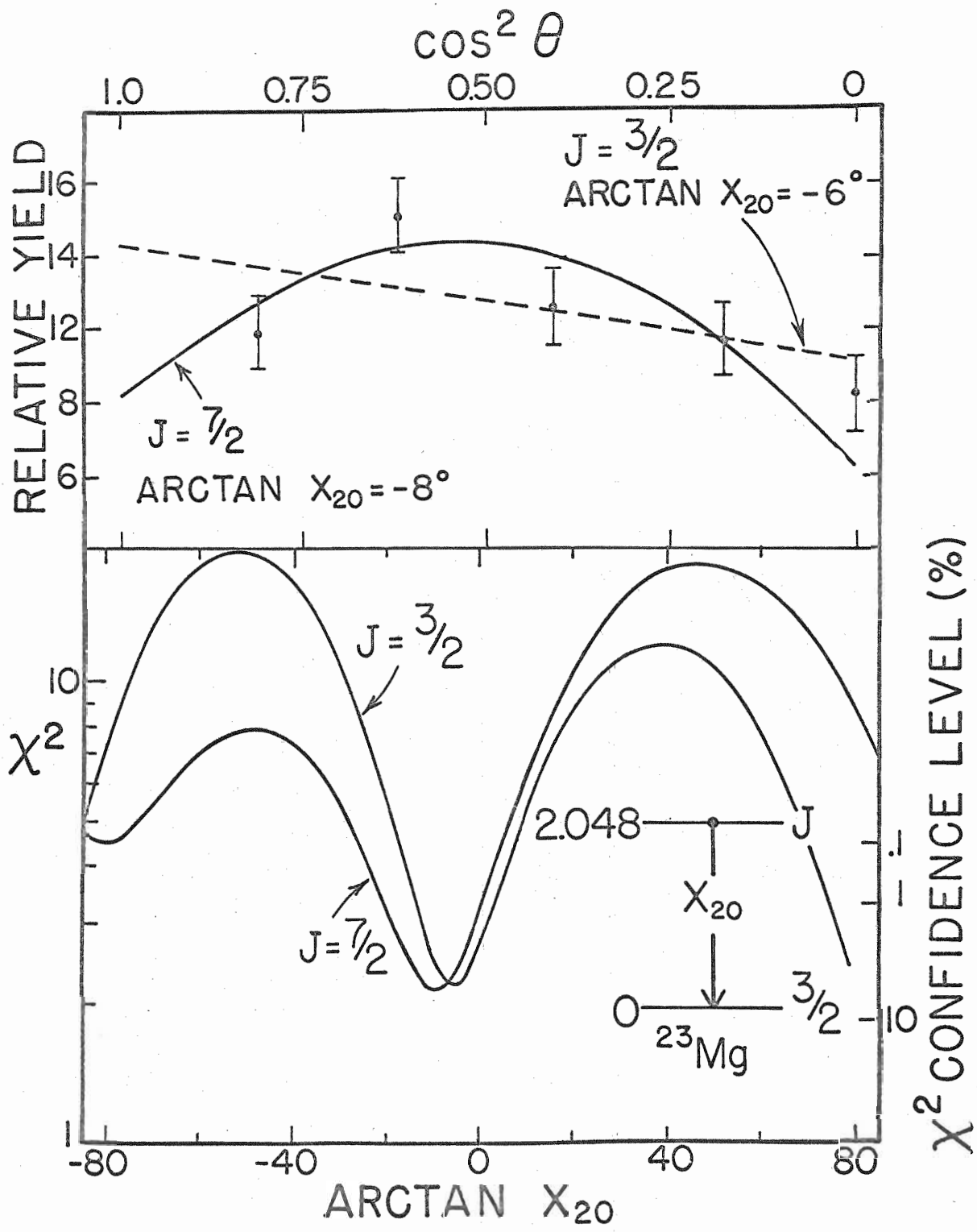
cos² θ
1.0
0.75
0.50
0.25
0
RELATIVE YIELD
16
14
12
8
6
J = 3/2
ARCTAN X20 = -6°
J = 7/2
ARCTAN X20 = -8°
χ²
10
1
J = 3/2
J = 7/2
2.048
J
X20
0
3/2
23Mg
-80
-40
0
40
80
ARCTAN X20
χ² CONFIDENCE LEVEL (%)
.1
10

The assumed analog of this level in ^{23}Na is the 2.08-MeV level. Poletti and Start (7) have studied the angular correlations from this level and find that J = 7/2 is the most probable spin for this level although J = 3/2 cannot be rigorously eliminated. If the ^{23}Na 2.08-MeV level and the ^{23}Mg 2.048-MeV level have positive parity, as suspected, then the mixing ratios x_{21} are E2 + M1 mixtures. For both J = 3/2 and 7/2 assignments to these two levels the mixing ratios x_{21} differ in sign for the corresponding transitions. The approximate rule for E2/M1 mixing ratios, discussed previously, does not in this case allow discrimination between spin assignments of 3/2 or 7/2 for the two mirror levels.

Considering all of the above information the spin of the 2.048-MeV level is most probably 7/2 although 3/2 cannot be rigorously excluded. The observed branching seems more consistent with J = 7/2 since with this assignment it is more likely that the 2.048-MeV level would decay strongly to the 0.451-MeV level with $\Delta J = 1$ than decay to the ground state with $\Delta J = 2$. The parity of the level is most likely positive since for a negative parity assignment the mixing ratio x_{21} for J = 7/2 would imply an improbably large M2 component in the 1.60-MeV radiation. Therefore $J^{\pi} = 7/2^{(+)}(3/2)$ for the ^{23}Mg 2.048-MeV level.

6. The 2.356-MeV Level

The 2.356-MeV level was studied at ^{3}He energies of 6.37 and 8.05 MeV. The coincident γ-ray spectrum, taken at 6.37 MeV and summed over five different angles, is shown in Figure 17. In analysing this

Figure 17. The 2.356-MeV Level Gamma-Ray Decay Spectrum. This figure illustrates the spectrum of γ rays in coincidence with the α group populating the ^{23}Mg 2.356-MeV level in the ^{24}Mg(^{3}He,$\alpha\gamma$)^{23}Mg reaction at a ^{3}He energy of 6.37 MeV. This spectrum is the sum of five spectra taken at five different angles to the beam. The γ-ray peaks correspond to the transitions indicated in the decay scheme. A 2.36-MeV spectral shape, shown sketched in, was used to extract the 1.91-MeV γ ray. Accidental coincidences have been subtracted.

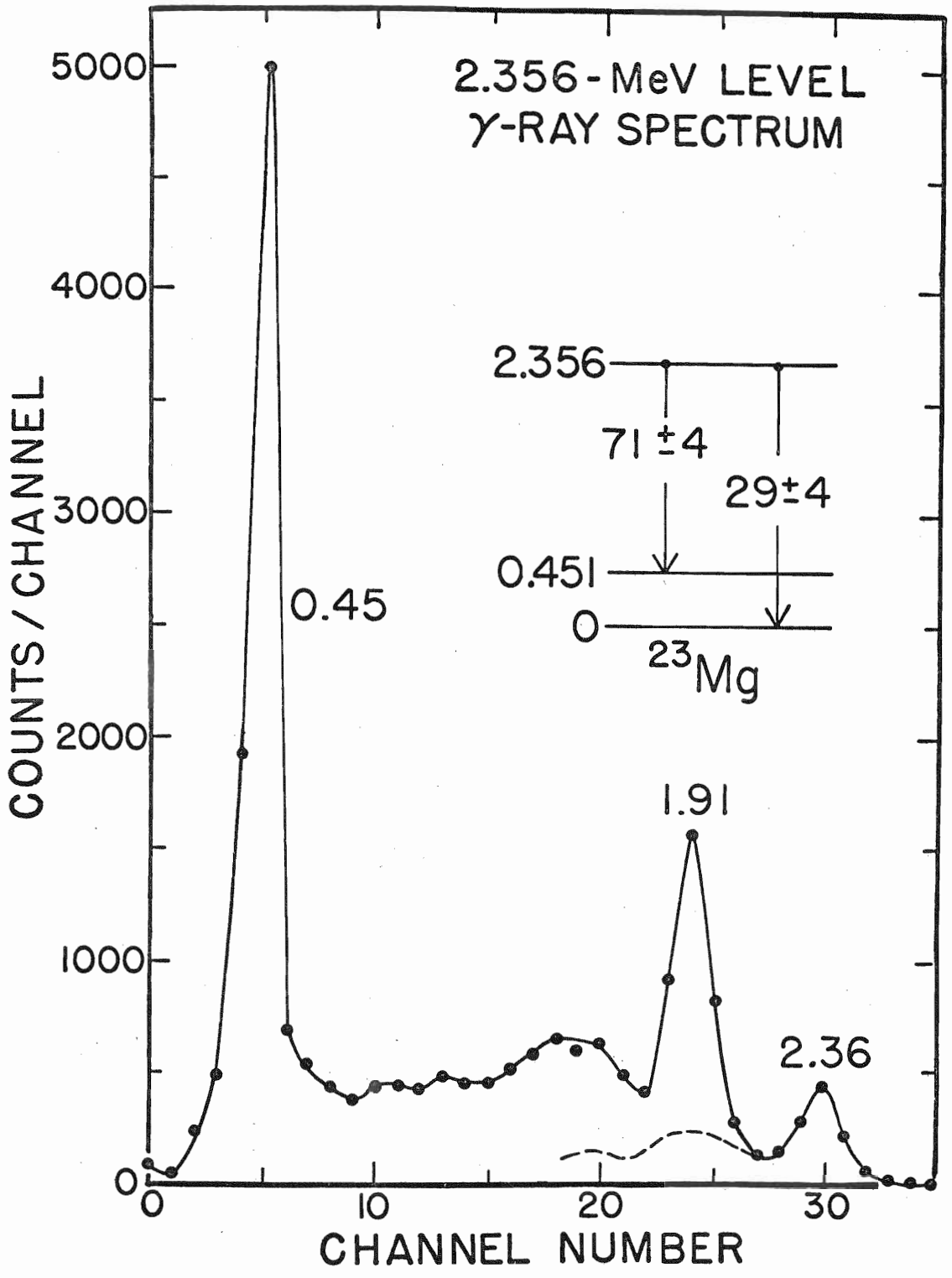
2.356-MeV LEVEL
γ-RAY SPECTRUM
COUNTS / CHANNEL
CHANNEL NUMBER
5000
4000
3000
2000
1000
0
0
10
20
30
0.45
1.91
2.36
2.356
71 ±4
29±4
0.451
0
23Mg

spectrum the 1.91-MeV γ ray was extracted using the 2.43-MeV γ ray from the $^{28}Si(d, p_3\gamma)^{29}Si$ as a spectral shape for the 2.36-MeV γ ray. The ^{29}Si 2.43-MeV level decays approximately 100% to the ground state. The ^{23}Mg 2.356-MeV level was found to decay to the ground and first excited state in the proportions (29 ± 4)% and (71 ± 4)%, respectively. These branching ratios were obtained from the a_o coefficients of the least-squares fit to the 2.36- and 1.91-MeV correlations. The errors in the branching ratios reflect both statistical uncertainty and the uncertainty in extracting the 1.91-MeV γ ray.

The spectrum of γ rays detected in the Ge(Li) detector at a ^3He energy of 8 MeV, and in coincidence with the α group leading to the 2.356-MeV level, revealed γ rays with energies of 0.453 ± 0.004 MeV, 1.909 ± 0.004 MeV, and 2.359 ± 0.004 MeV which could be identified with transitions from this level. The latter energy agrees with the value 2.356 ± 0.015 MeV given in Ref. 8 as the energy of the ^{23}Mg third-excited state.

The 2.36-MeV angular correlation, taken at a ^3He energy of 8.05 MeV, was characterized by $a_2/a_o = -0.01 \pm 0.05$ and $a_4/a_o = -0.03 \pm 0.08$. In applying the χ^2 test to this correlation the spin, J, of the 2.356-MeV level was assumed to range from 1/2 to 9/2. The χ^2 curves for these spin choices are illustrated in Figure 18. Acceptable solutions were found for J = 1/2 with x_{30} undetermined, J = 3/2 with $x_{30} = \tan(-15 \pm 8)^\circ (= -0.268 \pm 0.141$, or $\leq \tan(-79)^\circ (\leq -5.14)$, or $\geq \tan(81)^\circ (\geq 6.31)$, and J = 5/2 with $x_{30} = \tan(11 \pm 6)^\circ (= 0.194 \pm 0.105)$.

Figure 18. E_γ = 2.36-MeV Angular Correlation and χ^2 versus Arctan X_{30} for the 2.356-MeV Level. In the lower portion of the figure is illustrated the results of the χ^2 analysis of the 2.36-MeV angular distribution assuming the spin, J, of the 2.356-MeV level to be 1/2, 3/2, 5/2, 7/2, and 9/2. Acceptable solutions were found for J = 1/2 with x_{30} undetermined and J = 3/2 and 5/2 for specific multipole mixtures. The experimental angular correlation, taken at a ^{3}He energy of 8.05 MeV, is shown in the top portion of the figure. The solid line through these data is the fit for J = 1/2. The fits for J = 3/2 and 5/2 fit equally well. The percentages shown give the probability that a correct solution has a χ^2 of the corresponding value or larger.

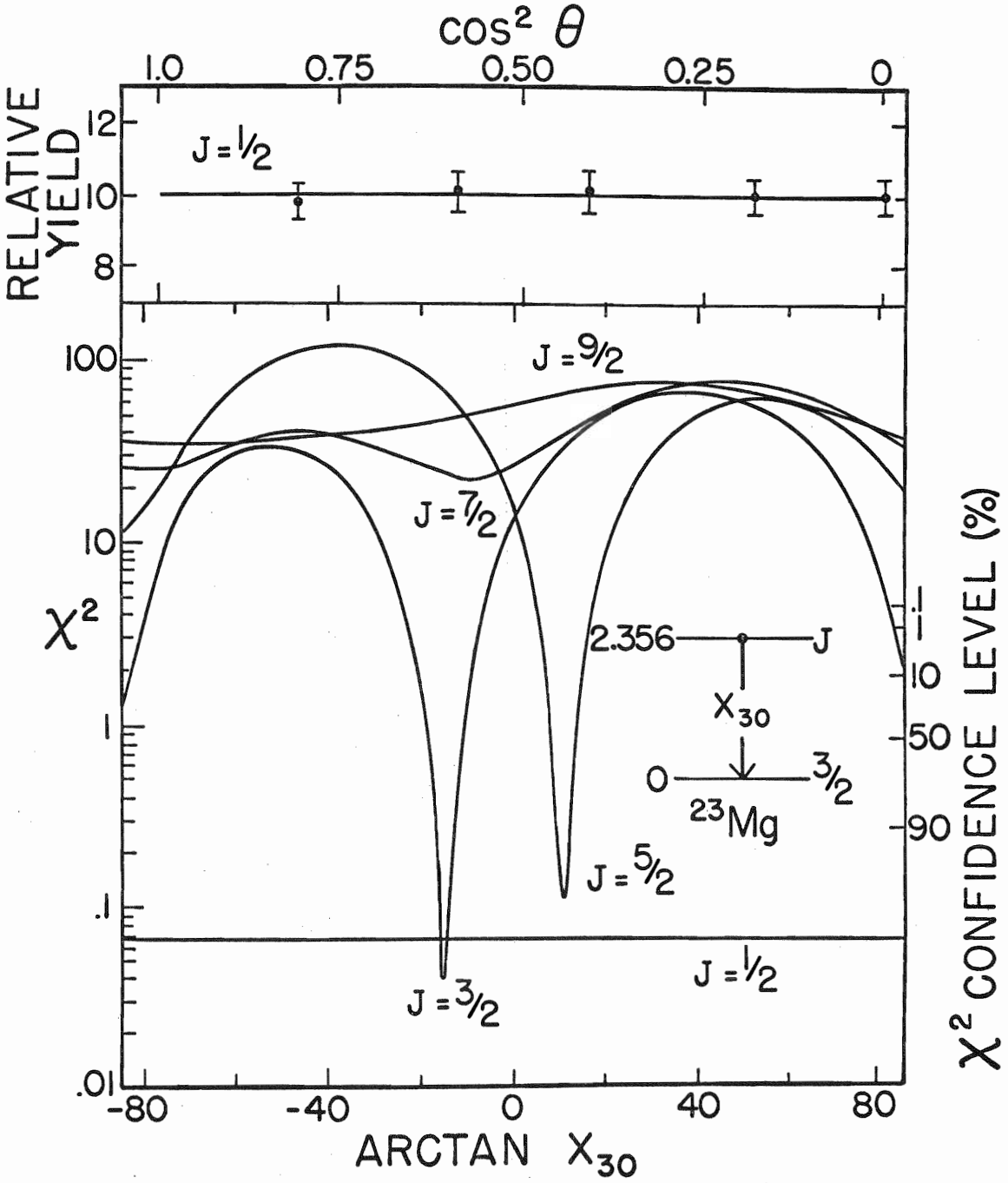
cos² θ
1.0
0.75
0.50
0.25
0
RELATIVE YIELD
12
10
8
J = 1/2
100
10
1
.1
.01
χ²
J = 9/2
J = 7/2
J = 5/2
J = 3/2
J = 1/2
2.356
J
X30
0
3/2
23Mg
-80
-40
0
40
80
ARCTAN X30
χ² CONFIDENCE LEVEL (%)
10
50
90

The 1.91-MeV correlation was extracted after subtracting the isotropic background of the 2.36-MeV γ ray. This correlation was characterized by $a_2/a_0 = 0.00 \pm 0.03$ and $a_4/a_0 = -0.03 \pm 0.04$. In the χ^2 analysis of this correlation the spin of the 2.356-MeV level was assumed to be J = 1/2, 3/2, and 5/2. The results of this analysis, shown in the left hand portion of Figure 19, lead to acceptable solutions of J = 1/2 with x_{31} undetermined, J = 3/2 with $x_{31} = \tan(-72 \pm 5)^\circ (= -3.08 \pm 0.09)$ or $\tan(-5 \pm 5)^\circ (= -0.087 \pm 0.087)$ and J = 5/2 with $x_{31} = \tan(-21 \pm 5)^\circ$ $(= -0.384 \pm 0.087)$.

The 0.45-MeV cascade correlation was extracted and was found to be characterized by $a_2/a_0 = 0.02 \pm 0.02$ and $a_4/a_0 = -0.03 \pm 0.03$. In applying the χ^2 test to this correlation, x_{31} was fixed at one of the values given above and arctan x_{10} was treated as a variable. The results of this analysis, shown in the right hand portion of Figure 19, show that only the solution for J = 1/2 yields a value of x_{10} for which the corresponding χ^2 has a confidence level of less than 0.1% within the allowed range of x_{10}. The solution for J = 3/2 with $x_{31} = \tan(-72)^\circ$ has a confidence level slightly above the 0.1% level within the allowed range. This analysis indicates that a spin of J = 1/2 for the 2.356-MeV level is approximately four times more probable than is a 3/2 assignment. For the latter spin the transition to the $J_1 = 5/2$, 0.451-MeV level must be largely quadrupole (i.e., $T_{31}(E2) = 9.5\, T_{31}(M1)$) if the parity of the level is positive. For negative parity and J = 3/2, the M2 transition strength would be improbably

Figure 19. E_γ = 1.91-, 0.45-MeV Angular Correlations and χ^2 versus Arctan X_{31}, Arctan X_{10} for the 2.356-MeV Level. The χ^2 analysis of the 1.91-MeV correlation, with the results illustrated on the left, was made assuming the spin, J, of the 2.356-MeV level to be 1/2, 3/2, and 5/2. The spin of the 0.451-MeV level was fixed at $J_1 = 5/2$. Each of these spin choices is seen to yield acceptable solutions, the 3/2 and 5/2 choices for specific mixtures x_{31}. The top portion of the figure shows the experimental data taken at a ^{3}He energy of 8.05 MeV. The solid line through these data is the fit for J = 1/2. The results of analysing the 0.45-MeV cascade correlation (with x_{31} fixed at the values found from analysing the 1.91-MeV correlation) is illustrated on the right. Only J = 1/2 yields a consistent value of x_{10} with a confidence level less than 0.1%, the solution with J = 3/2 and $x_{31} = \tan(-72)^\circ$ being slightly above the 0.1% confidence level. The experimental data is shown at the top of the figure along with the fit for J = 1/2.

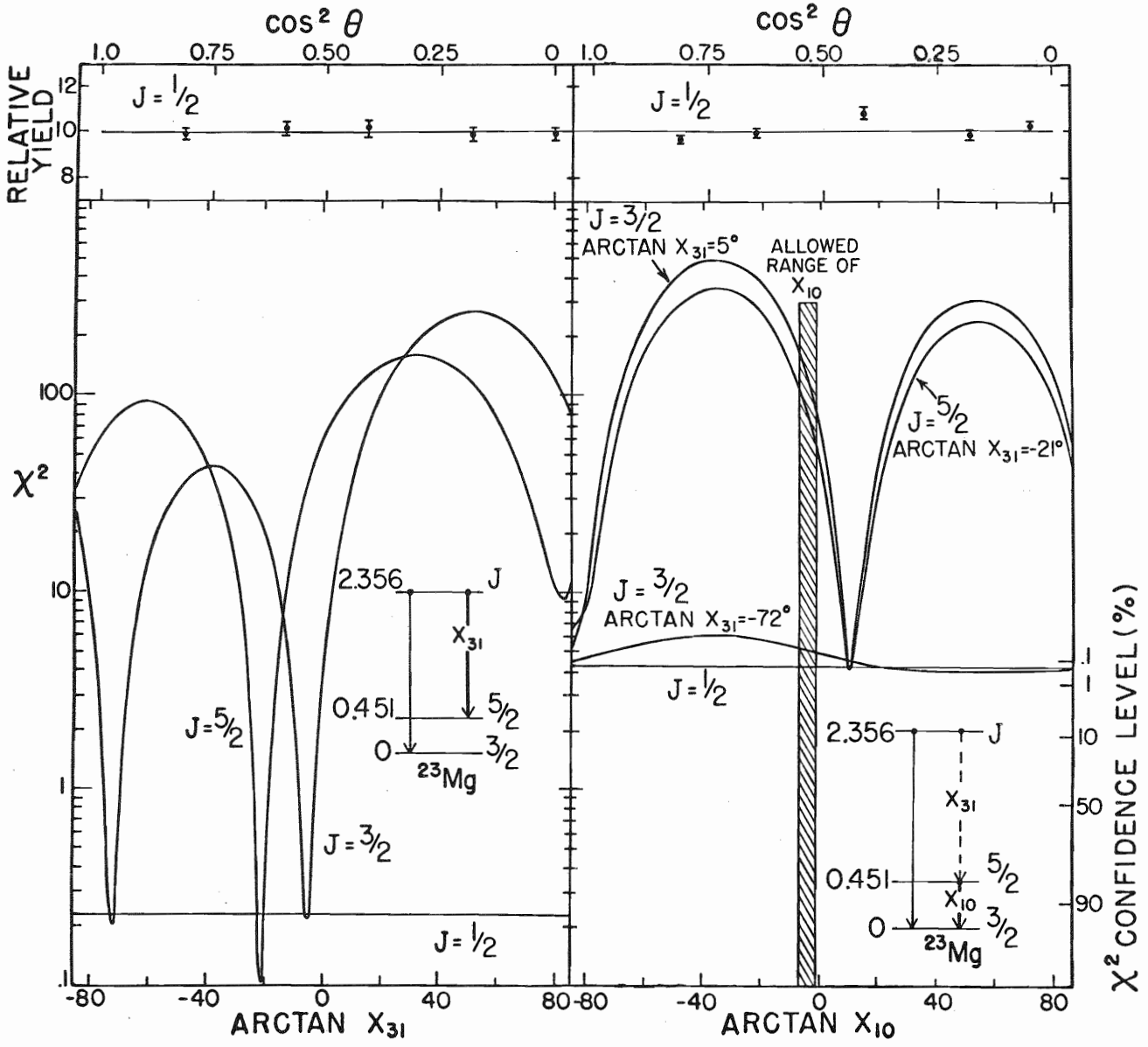
cos² θ
1.0
0.75
0.50
0.25
0
RELATIVE YIELD
12
10
8
J = 1/2
J = 1/2
J = 3/2
ARCTAN X31=5°
ALLOWED RANGE OF X10
J = 5/2
ARCTAN X31=-21°
J = 3/2
ARCTAN X31=-72°
J = 1/2
χ²
100
10
1
.1
J = 5/2
J = 3/2
J = 1/2
2.356
J
X31
0.451
5/2
0
3/2
23Mg
2.356
J
X31
X10
0.451
5/2
0
3/2
23Mg
-80
-40
0
40
80
ARCTAN X31
ARCTAN X10
χ² CONFIDENCE LEVEL (%)
10
50
90

large.

Strong support for the $J = 1/2$ assignment comes from the work of Joyce et al. (16) and Dubois and Earwaker (24) who found the a_3 angular distribution from the $^{24}Mg(^3He, a)^{23}Mg$ reaction to be characterized by an $\ell_n = 0$ pickup pattern. In addition, Ganguly et al. (17) and Kozub (18) found the d_3 angular distribution to also be characterized by $\ell_n = 0$. The 2.356-MeV level thus has an unequivocal $J^\pi = 1/2^+$ assignment as was favored from the analysis of the angular correlations from this level.

The assumed mirror level in ^{23}Na is at 2.39 MeV. Dubois (56), using the $^{22}Ne(^3He, d)^{23}Na$ reaction, has found the d_3 angular distribution to be well fitted with an $\ell_p = 0$ pickup pattern which leads to a $J^\pi = 1/2^+$ assignment to this level. Richter and von Witsch (57), in a different experiment, also report $J^\pi = 1/2^+$ for this level. Poletti and Start (7) have studied the angular correlations from this level and concluded that $J = 1/2$ (3/2).

7. The 2.712- and 2.768-MeV Levels

The 2.712-MeV level was studied in conjunction with the 2.768-MeV level as it was impossible to separately resolve the a groups populating these levels using only a semiconductor detector. A magnetic spectrometer would have been required as was employed by Dubois and Earwaker. (24) A ^3He energy of 8.05 MeV was used to populate these levels as at this energy the close-lying 2.904-MeV level was weakly populated (see Fig. 3).

In order to determine the decay modes of these two levels a

spectrum of the γ rays detected in the Ge(Li) counter and in coincidence with the α groups leading to the 2.712-, 2.768-, and 2.904-MeV levels was taken. This spectrum, recorded at a ^{3}He energy of 8 MeV, is shown in Figure 20. A three-point running average has been made of the data illustrated in this figure. The energies of the γ-ray peaks shown were obtained using the ^{24}Na calibration curve discussed in Chapter II. In obtaining this spectrum three TPH intervals were used as previously discussed. The slanted lines at channels 400 and 800 in the figure are the boundaries of the three γ-ray spectra which were obtained for the different TPH intervals. Accidental coincidences have not been subtracted from the spectrum although this will not affect the conclusions drawn. Gamma rays with energies of 2.767 ± 0.004 MeV and 1.751 ± 0.004 MeV (double escape peak) can be identified with a ground state branch from the 2.768-MeV level. These two energies agree with the result 2.768 ± 0.010 MeV given in Ref. 8 for the energy of the fifth-excited state. Gamma rays with energies of 2.261 ± 0.006, 0.451 ± 0.004, 0.661 ± 0.004, and 1.603 ± 0.005 MeV can be identified with transitions from the 2.712-MeV level through the first and second excited states as indicated in the decay scheme. There is no evidence for a ground state branch from the 2.712-MeV level. The two energies 2.261 and 0.451 MeV lead to an energy of 2.712 ± 0.007 MeV for the fourth excited state in agreement with the result 2.712 ± 0.010 MeV given in Ref. 8. Gamma rays with energies of 2.902 ± 0.008, 2.454 ± 0.008, and 0.451 ± 0.004 MeV can be identified with transitions from the

Figure 20. The 2.712-, 2.768-, and 2.904-MeV Level Gamma-Ray Decay Spectrum Recorded with the Ge(Li) Detector. This figure illustrates the spectrum of γ rays taken at $\theta = 90^{\circ}$ to the beam with the Ge(Li) detector, and in coincidence with the α groups leading to the ^{23}Mg 2.712-, 2.768-, and 2.904-MeV levels in the ^{24}Mg(^{3}He, $\alpha\gamma$)^{23}Mg reaction at a ^{3}He energy of 8 MeV. The γ-ray peaks correspond to the transitions indicated in the decay scheme. The branching ratios given in the decay scheme were found from a summed γ-ray spectrum taken with a NaI crystal. The energies in the decay scheme are from Ref. 8 whereas the energies of the γ-ray peaks in the figure were deduced from a ^{24}Na calibration curve. A three-point running average has been made of the data illustrated here. Accidental coincidences have not been subtracted. See the accompanying text and Section B of Chapter II for further details.

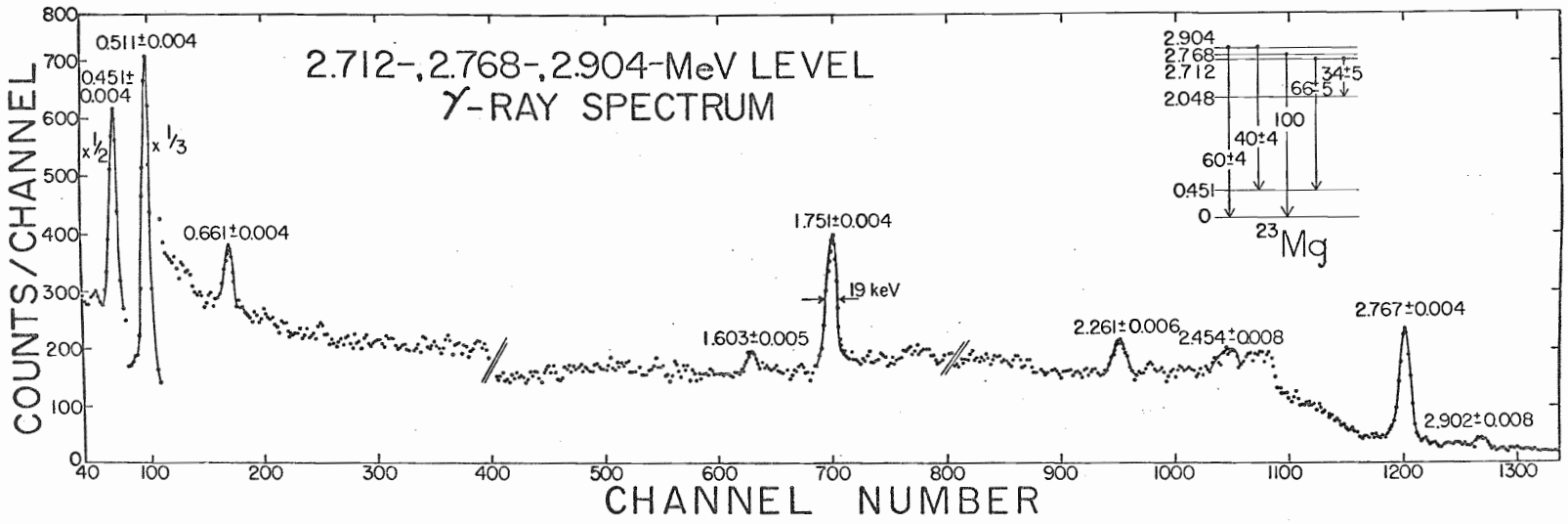
2.712-, 2.768-, 2.904-MeV LEVEL
γ-RAY SPECTRUM
COUNTS/CHANNEL
CHANNEL NUMBER
0.511±0.004
0.451±0.004
x 1/2
x 1/3
0.661±0.004
1.751±0.004
19 keV
1.603±0.005
2.261±0.006
2.454±0.008
2.767±0.004
2.902±0.008
2.904
2.768
2.712
2.048
0.451
0
66±5
34±5
100
40±4
60±4
23Mg

decay of the 2.904-MeV level. In conclusion, this spectrum is consistent with the assumption that the 2.768-MeV level decays 100% to the ground state and that the 2.712-MeV level decays only through the first and second excited states. The statistics are low and weak branches may have been missed.

Using these decay modes the branching ratios were determined from the spectrum of these γ rays detected in the NaI counter. A typical NaI spectrum is shown in Figure 21. From a summed γ-ray spectrum it was found that the 2.712-MeV level decays (66 ± 5)% to the 0.451-MeV level and (34 ± 5)% to the 2.048-MeV level. In obtaining these branching ratios a 2.75-MeV γ ray from a ^{24}Na source was used as a spectral shape for the 2.77-MeV γ ray to extract the 2.26-MeV γ ray. This shape is shown dashed in Figure 21. An approximate flat-line background was subtracted in extracting the 0.66-MeV γ ray as shown in the figure. The error in the branching ratios reflects both statistical uncertainty and the uncertainty in extracting the 0.66- and 2.26-MeV γ rays.

The 2.77-MeV correlation was characterized by $a_2/a_0 = 0.00 \pm 0.01$ and $a_4/a_0 = 0.00 \pm 0.02$. The results of the χ^2 analysis are shown in Figure 22. The observed isotropy is consistent with solutions of J = 1/2 with x_{50} undetermined, J = 3/2 with $x_{50} = \tan(-14 \pm 2)^\circ (= -0.249 \pm 0.035)$ and J = 5/2 with $x_{50} = \tan(11 \pm 2)^\circ (= 0.194 \pm 0.035)$. The absence of branching to the 0.451-MeV level favors a J = 1/2 assignment. If the parity of the 2.768-MeV level is positive then the ratio of transition

Figure 21. The 2.712-, 2.768-MeV Level Gamma-Ray Spectrum Recorded with the Na(Tl) Detector. This figure illustrates the spectrum of γ rays taken at $\theta = 50^{\circ}$ to the beam with the Na(Tl) detector, and in coincidence with the α particles leading to the ^{23}Mg 2.712- and 2.768-MeV levels in the ^{24}Mg(^{3}He, $\alpha\gamma$)^{23}Mg reaction with a ^{3}He energy of 8.05 MeV. The γ-ray peaks correspond to the transitions indicated in the decay scheme deduced from the Ge(Li) detector spectrum. A 2.77-MeV spectral shape, shown sketched in, was used to extract the 2.26-MeV γ ray. The manner in which the 0.66-MeV γ ray was extracted is also indicated. The branching ratios were deduced from a NaI γ-ray spectrum summed over four different angles to the beam. Accidental coincidences have been subtracted from the spectrum shown here.

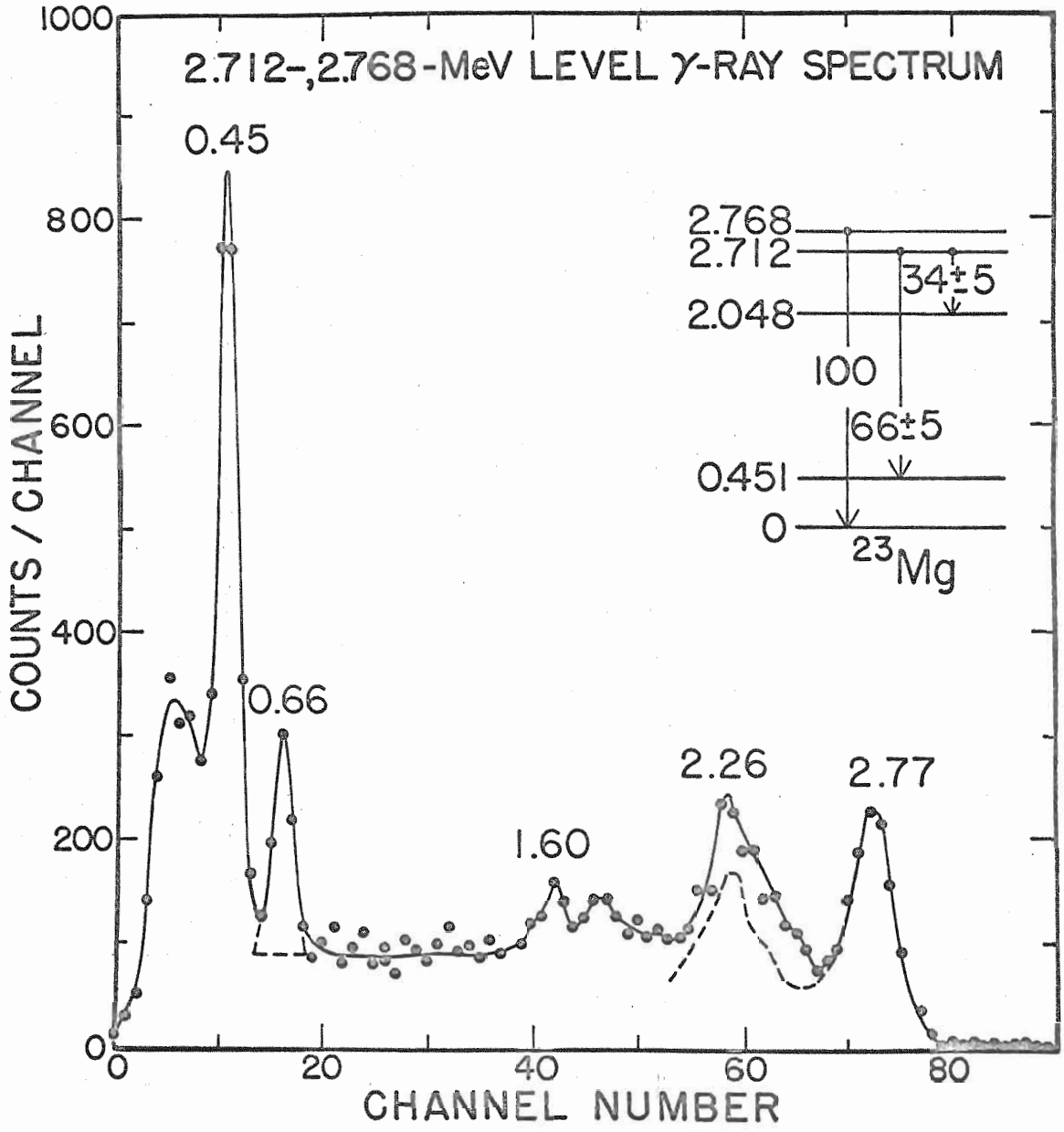
2.712-,2.768-MeV LEVEL γ-RAY SPECTRUM
0.45
0.66
1.60
2.26
2.77
2.768
2.712
2.048
0.451
0
34±5
100
66±5
23Mg
COUNTS / CHANNEL
CHANNEL NUMBER
1000
800
600
400
200
0
0
20
40
60
80